2a

AIAA ELECTRIC PROPULSION CONFERENCE
BROADMOOR HOTEL, COLORADO SPRINGS, COLO. MARCH 11-13, 1963





# COMPARISON OF COMMERCIAL, SPHERICAL POWDER AND WIRE BUNDLE TUNGSTEN IONIZERS

G. Kuskevics and B. L. Thompson

AIAA 63016

## DISCLAIMER

# COMPARISON OF COMMERCIAL, SPHERICAL POWDER AND WIRE BUNDLE TUNGSTEN IONIZERS[1]

G. Kuskevics and B. L. Thompson

ABSTRACT

Cesium ionization on different porous tungsten structures was measured in terms of neutral fraction, critical temperature, and flow rate in a regular laboratory test chamber environment in the $10^{-6}$ torr range. These structures included 3/16" commercial sintered ionizers with about 2 micron average pore diameter, spherical powder ionizers[2] of 6 micron effective pore diameter and, 12 and 6 micron diameter wire bundle ionizers[3].

Conductance was measured at room temperature with nitrogen and at operating temperature with cesium vapor. The neutral fraction was obtained by a surface ionization probe measurement at $15^{\circ}$ to the beam axis. The angular distribution of cesium atom efflux in the non-ionizing state without accelerating voltage was assumed to be the same as that of the neutral efflux in the ionizing state with accelerating voltage applied. This assumption was checked out experimentally by means of a surface ionization atom probe which could be moved in a circular arc with the ionizer at the center. Critical temperatures were derived from the ion current versus ionizer temperature curves. The ion current was measured at a liquid nitrogen cooled, grooved current collector which had two grids to

---

1 Performed under Contracts AF33(616)-6958, NAS8-2547, and NAS8-1537

2 Developed by H. Todd and M. LaChance of Electro-Optical Systems, Inc. under NASA Contract NAS8-2547

3 Developed by H. Todd of Electro-Optical Systems, Inc. under NASA Contract NAS8-1537

suppress secondary electrons. The ionizer temperature was measured with a sheathed tungsten-rhenium alloy thermocouple.

Ion current and neutral fraction were plotted as log j or log $\alpha$ versus 1/T which allowed easier selection of the critical temperatures. The directly heated ionizers could be operated up to 1500°C. In general the performance of ionizers improved with time of operation. During this conditioning time the critical temperature and neutral fraction shifted to lower values. The best critical temperatures for all tungsten ionizers in the $10^{-6}$ torr residual gas pressure at current densities between 1 and 20 ma/cm$^2$ were within 100°K of Langmuir's data for solid tungsten. Since the surface was not clean the critical temperature had a considerable spread.

Neutral fractions for commercial sintered, spherical powder and fine wire bundle ionizers ranged from 0.1 to 5 percent, but were considerably higher for coarse wire bundle ionizers. The angular distribution measurements of neutral fraction were used to select the best angular position of a neutral efflux detector for neutral fraction measurements and to test the validity of the assumption that the relative angular distribution remains independent of whether a beam is being extracted.

## 1. REVIEW OF SURFACE IONIZATION ON POROUS TUNGSTEN

The first practical cesium ionizers in the early ion sources, surface ionization detectors and even ion propulsion devices used solid tungsten filaments or ribbons. Surface ionization of the alkali metals on solid refractory metal surfaces has been reviewed recently by Zandberg and Ionov (Ap59ZI). A brief review of surface ionization on other solid materials was given previously (Mr62KS4).

Studies of porous ionizers started with the application of commercial porous tungsten in ion engines in late 1958 (De58BD6, Au59FS). At the same time theoretical studies of surface ionization on idealized porous structures determined that the desirable pore size should be less than 1 micron (Au59FS, No60ZST, No60NS, Au61RK).

More basic experiments with porous ionizers were performed only later. The first of these by Stavisskii and Lebedev (Oc60SL) used a relatively large (10 mm dia, 2 mm thick) porous tungsten disc of 70% of theoretical density, made of a very fine 1 micron grain size. Several Pt-Pt/Rh thermocouples inside of the porous disc were used to determine the surface temperature by extrapolation to within $\pm 1^{\circ}$ for calibration of the heater and the optical pyrometer. Temperature varied from 1050 to 1000°C across the thickness of the ionizer. The temperature variations along the radius of the surface is less than 3°C. The ion current was measured by a water-cooled Faraday collector with a secondary electron suppressor. The Faraday cup collector was also the accelerator electrode with its aperture about 7 mm from the ionizer. Thus sputtering of cesium and the unidentified collector material could reach the ionizer since there was no baffling to minimize it.

The ion current-ionizer temperature curves were similar to those for solid tungsten illustrated in Fig. 23, Section 9. Following the definitions of different regions of surface ionization in Fig. 24 of Section 9, the ion current in the low coverage region was constant suggesting near 100% ionization. The critical temperature $T_{CI}$ was 80° above Langmuir's data for solid tungsten at 10 ma/cm$^2$ and 50° higher at 0.25 ma/cm$^2$. The pressure was not specified but an apparatus diagram suggests an untrapped oil diffusion pump system with operation in the $10^{-6}$ torr range.

More extensive studies of porous tungsten ionizers at pressures below $10^{-7}$ torr were reported by Husmann (Mr62Hus). Operation in a bakable, mercury and ion pumped glass system in the $10^{-8}$ torr region after a short flash of the ionizer at 1700°C produced a "clean" surface. The ionizer temperature was measured by a pyrometer and the neutral fraction by a 1.25 cm$^2$ area probe located 6" away but on the ionizer axis. The ion beam was deflected electrostatically to a $LN_2$ cooled collector (Au61HRL). The ion current-temperature curves

for fine porous discs (~ 2 μ pore dia) were reproducible and the critical temperatures at 10 ma/cm$^2$ were only 40 to 80°K above Langmuir's data for solid tungsten. For coarse discs (My62HRL) or fine oxidized discs (No61HRL) the critical temperatures were about 150°K higher than Langmuir's. The neutral fractions for clean, fine discs ranged from 0.5-2 % at 1 ma/cm$^2$ to 7-9 % at 10 ma/cm$^2$. For oxidized discs the neutral fractions were 1/3 lower. Oxidation was provided by admitting oxygen to raise the total pressure to $10^{-6}$ - $10^{-5}$ torr.

Emissivity of sintered tungsten was measured as a function of pore size. The emissivity increased with temperature from 100-200°C with a slope similar to that of solid tungsten. The emissivity of discs made of 0.9 - 18 micron powder at 1200°C ranged from .25 to .55 independently of powder size (Au61HRL). Mass spectroscopic analysis of the residual gas at $10^{-7}$ torr indicated the presence of $H_2$, $N_2$ and $H_2O$ but no $O_2$ or $CO_2$. The sensitivity was sufficient to give an indication at 2 x $10^{-9}$ torr. (My62HRL).

The first attempt to study surface ionization as a function of ionizer grain size (or structure) gave ionization efficiencies of 94 and 97% for ionizers made of 5 and 8 micron powder, respectively. Since no ion current density, critical temperature or emissivity were given, this work could not be compared with that of other investigators (Jn61HS). The atom and ion emission from a much larger 1" dia porous tungsten ionizer was studied by H. Shelton (Mr62She) using a tantalum ribbon neutral sensor. At $10^{-6}$ torr and ion current densities of about 0.5 ma/cm$^2$, the neutral fraction ranged from 0.2 to 3%. The tungsten was often oxygenated and some cases of poisoning were observed.

Some data by the above investigators are included in the graphs of the final section.

## 2. IONIZER PERFORMANCE CRITERIA

The important ionizer performance criteria are ionization efficiency, ion generation energy efficiency and lifetime as

as discussed in detail by Kuskevics (Ja62Kus). Since the ionization efficiency is usually very close to 100 percent, accuracy is obtained by measuring the neutral fraction, defined as the ratio of neutral cesium efflux to total cesium efflux. The ion generation energy efficiency is a measure of thermal losses due to radiation from the ionizing surface, radiation and conduction losses from the supporting structure and leads. For evaluation of the ionizer material only the thermal radiation from the ionizing surface is of importance. However, in a small single-button device other losses predominate. The radiation loss from the active area is best obtained by measurement of the minimum operating temperature and the total emissivity. The minimum operating temperature is equal to the so-called critical temperature. For porous tungsten ionizers in $10^{-6}$ torr vacuum, most good ionizers have a rather sharp critical temperature and a very small difference between the lower and upper critical temperature (hysteresis) determined from the ion current-ionizer temperature curve. For many ionizers, ion current starts a sharp decline at the same time as the neutral fraction starts to rise. Some ionizers, however, showed a minimum in neutral fraction at a temperature higher than the critical temperature for the ion current. The ion current critical temperature, $T_{CI}$, is most conveniently defined as that temperature at which the current has decreased by 5 percent from its maximum value. This is discussed in more detail below.

The total emissivity can be measured in a separate experiment using the same material. It is assumed here that the differences in emissivity are smaller than the effect of the spread in the critical temperatures and that they would favor high emissivity ionizers.

Some indication concerning the life of the ionizers can be obtained by observing time trends in their gas and cesium permeability, neutral fractions and critical temperatures. Only limited data were obtained because of the short duration of most tests. Most of these tungsten ionizers could be operated for over 100 hours

between 1400 and 1500°C without any decrease of permeability.

## 3. IONIZER TEST APPARATUS

Nearly all ionizers tested were discs of 3/16 inch diameter x .040 inches thick. They were brazed into a molybdenum holder, as shown in Fig. 1 and 2, using a Mo-C-B braze. This ionizer assembly was mounted into a single-aperture ion accelerator using a 45° beam-forming electrode and planar accel-decel electrodes, as shown in Figs. 3 and 4. The electrode geometry was similar to that of the multi-aperture ion engines. The electrode alignment was done visually to within about ± .020 inch. The temperature of these copper electrodes is lower than that in the multi-button engines because of the larger area for radiation.

A few grams of cesium were loaded into the reservoir using regular dry box techniques. The oxygen content of the cesium was not known. Upon removal of the ionizer assembly from the dry box, the cesium in the reservoir was under one atmosphere pressure of nitrogen. The low permeability of the porous ionizer was the only barrier against the infusion of air while the assembly was mounted into the accelerator and transferred into the vacuum test chamber.

The ionizer-accelerator assembly was placed in a 1 x 3 foot vacuum tank which was equipped with either a stationary or a movable neutral detector, a liquid-nitrogen cooled ion collector and a liquid-nitrogen-cooled liner. Operating pressure was usually between $2 \times 10^{-6}$ and $2 \times 10^{-5}$ torr. A schematic view of the neutral eye is also shown in Fig. 3, the ion collector in Fig. 5. The ionizer temperature was measured by a W5%Re-W26%Re thermocouple in a 1/16 inch OD tantalum sheath. The hot junction was in a deep hole in the ionizer holder and very near to the ionizer disc. The other end of the thermocouple passed through the vacuum wall without interruption by means of a gasketed feedthrough.

The reservoir temperature was monitored by a bare iron-constantan thermocouple near the exit of the massive nickel reservoir. Both

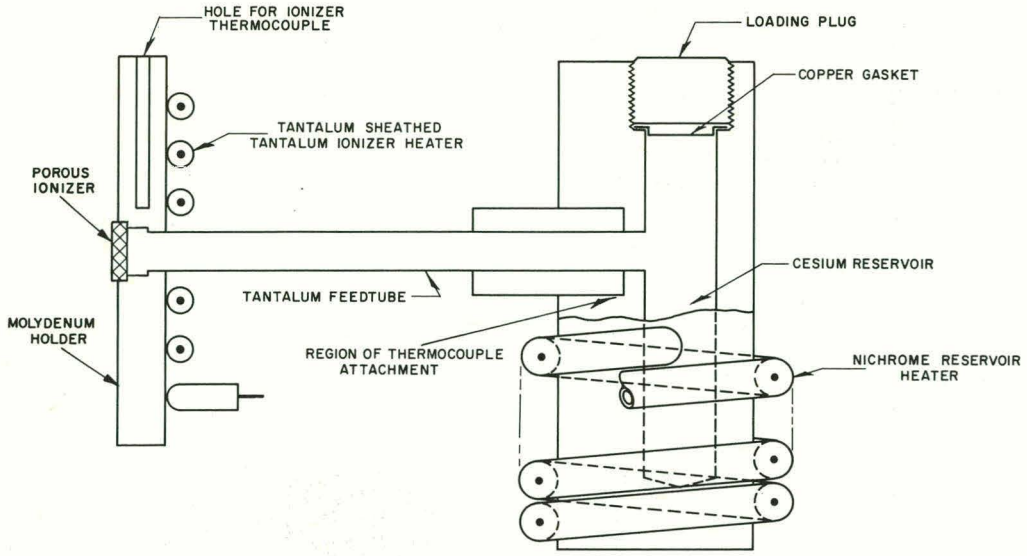


FIG. 1

SCHEMATIC OF THE IONIZER-RESERVOIR ASSEMBLY

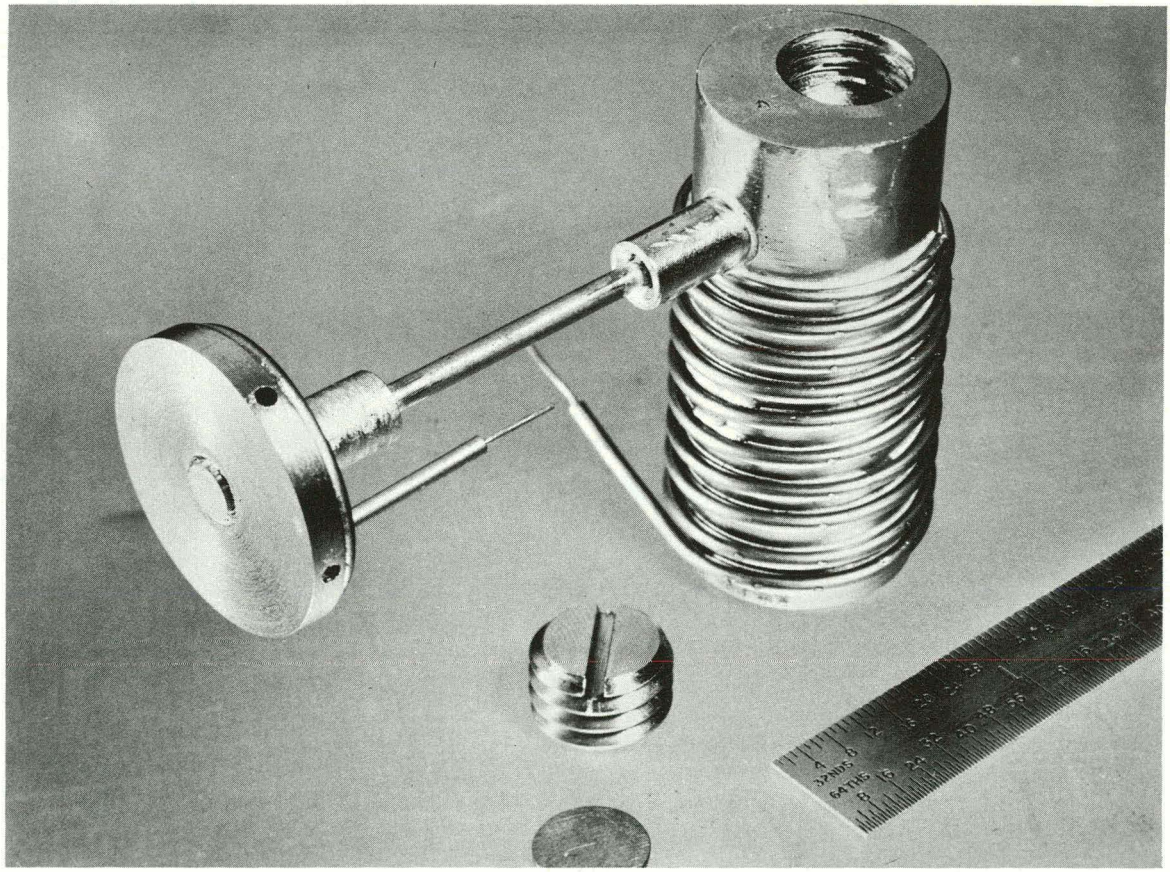

FIG. 2 IONIZER RESERVOIR ASSEMBLY

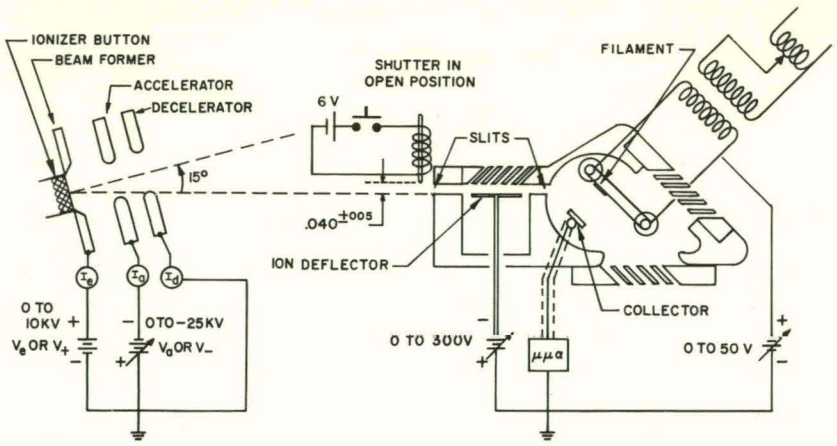


FIG. 3

SCHEMATIC AND CIRCUIT DIAGRAM OF ION ACCELERATOR AND NEUTRAL DETECTOR

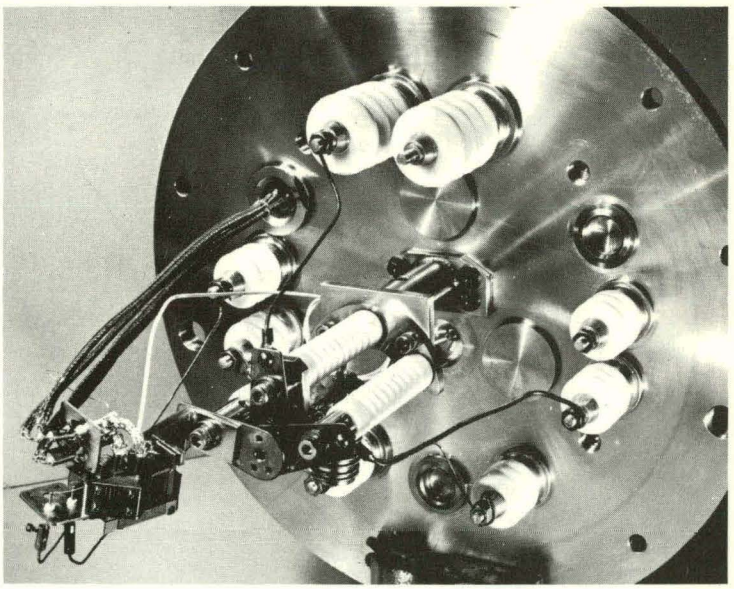

FIG. 4 IONIZER TESTING EQUIPMENT INCLUDING NEUTRAL DETECTOR

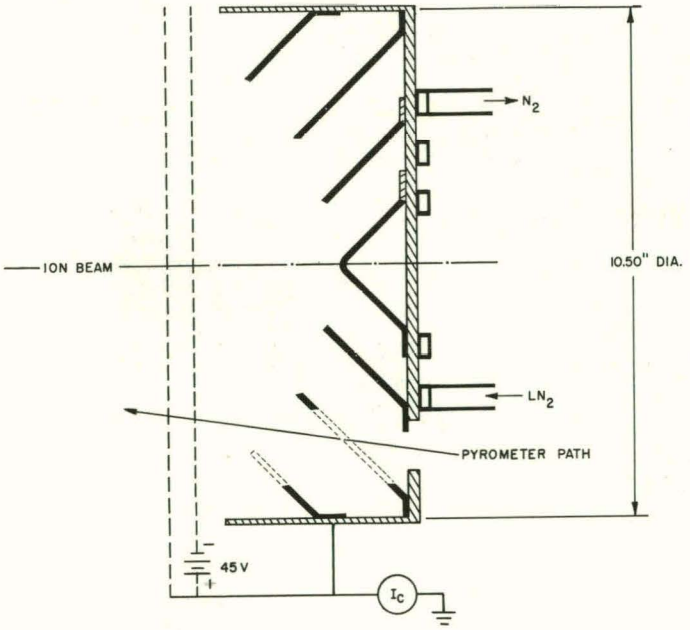


FIG. 5 CONICAL BAFFLE CURRENT COLLECTOR WITH ELECTRON IMPRESSION

temperatures were recorded on a 2-channel stripchart recorder which was isolated for operation at high voltage. Current meters were used in the ionizer and accelerator electrode circuits. A 90 v secondary electron suppression voltage was applied to the current collector. The ion current and neutral probe current were recorded on a 10-channel sampling chart recorder.

4. IONIZER TEST PROCEDURE

The gas conductance of most ionizers was measured before and after brazing into the holder and again after the ionizer tests. The ionizer and reservoir heaters were turned on at the same time as all instrumentation and high voltages. The neutral eye filament was baked out at 1600°C until the background reading with the shutter closed was a few nanoamps. The operating temperature was between 1100-1300°C depending upon atom incidence rates. The ionizer was heated to about 1300°C.

The ion collector current was monitored to establish the proper cesium-reservoir temperature for a reasonable ionizer current density, say, 5 ma/cm$^2$. With the reservoir temperature and cesium flow stabilized, the accelerator/ionizer voltage ratio for proper focusing was checked visually by observing the ion beam impact area at the collector or by observing the beam at $10^{-5}$ torr of argon. Usually the accelerator voltage was twice the magnitude of the ionizer voltage and the beam was 1 - 2 inches in diameter at the collector.

With proper focusing, the current-voltage characteristic was taken to insure emission-limited operation. This was done for each new current density and is very important at the high current densities when operation is very near to being space charge limited. The movable neutral detector was usually located at 15° to the ion-beam axis and 6 inches from the ionizer. The detector had .020 inch wide slits. The stationary detector had .040 inch slits and was only 3 inches from the ionizer. If the neutral fraction was below 10 percent, indicating that the ionizer had been properly conditioned, the angular dependence of $\alpha$ was checked to see that it was fairly

constant and that the probe was located at the proper angle for reliable results. Operation too close to the beam or too much in the shadow of the electrodes gave erroneous results.

The neutral fraction was obtained by measuring the neutral detector current with accelerating voltages on and off, subtracting background readings obtained by operating the shutter. After the proper probe angle was checked, the ion current and neutral fraction was measured as a function of ionizer temperature for a series of current densities. The dependence of cesium permeability upon the ionizer temperature was also obtained since it is related to the ion current density j. The j vs $T_e$ curves were taken repeatedly to observe reproducibility, hysteresis, and time trends.

After each test, the ionizer was inspected and its nitrogen conductance checked. Three types of tungsten ionizer structures were tested: 1) commercial sintered ionizers designated by the symbol SW, 2) spherical powder ionizers designated SP, and 3) wire bundle ionizers designated WB.

## 5. IONIZER NITROGEN CONDUCTANCE PERMEABILITY, AND BRAZE INFILTRATION

Nitrogen conductance measurements using electronic timer equipment provided a fast and simple method to check and sort large numbers of unmounted porous ionizers. The actual measurement determined the time for the pressure in a constant volume to drop about 1 percent of the pressure difference across the ionizer. The inverse of this time is proportional to the conductance of the sample. Conductance depends both upon the area and the thickness. Both can be easily measured for unmounted ionizers and used to calculate permeability. The permeability value is independent of sample area and thickness and depends only upon the material. The distribution of permeability for a large number of ionizers is indicative of the ionizer material uniformity. The gas permeability is a much more sensitive indicator of material quality than apparent material density. Change in permeability with time at high temperature

provides an indication of structural instability. For ionizers brazed into a holder the open area is no longer definite due to braze infiltration and it is impossible to calculate gas permeability. One can assume that the permeability of an unmounted ionizer does not change during brazing, if the brazing temperature is considerably lower than the sintering temperature.

The nitrogen conductance was checked before performance testing. These tests are also useful for the detection of leaks after brazing, cracks upon testing, braze penetration, or changes of permeability. Care must be taken to remove all cesium, its oxides and cleaning fluid from the ionizer after testing, since these can effectively seal the ionizer pores. Most ionizers were baked out in vacuum after their performance testing.

The conductance was measured before and after brazing the ionizer into a holder. The permeability was calculated from the unmounted ionizer measurement. An apparent permeability was calculated for the mounted ionizer, using the same area and thickness value. The ratio of the true and apparent permeability then gives the ratio of initial to effective post brazing area. Table I shows true permeability, apparent permeability before and after performance testing, and the closed area fraction and cesium-permeability represented by j at 300°C for the SP ionizers. From this table the fraction of ionizer area closed by brazing varies from 46-74% with an average 55% closure. The ionizer holder produces a braze infiltration pattern as shown in Fig. 6 and Table II. From Fig. 6 and the column of porous area one can see the extensive braze infiltration at the rear surface. The gas conductance should be determined by the average cross sectional area near the center of the ionizer. The braze closure varies from 12 percent at the front surface to 50 percent at the rear surface, while the gas conductance closure was 46 percent. Hence, the gas conductance is more determined by the minimum open cross section than by a geometric average.

TABLE I

TRUE AND APPARENT PERMEABILITY FOR SPHERICAL POWDER IONIZERS

| Ionizer Identity | True permeability $K = \frac{\Delta m}{\Delta p}\frac{\Delta x}{A}\frac{1}{\Delta t}$ g/(cm·torr·sec) $\Delta x/A = .5705$ | Apparent permeability after brazing $K_1$ g/(cm·torr·sec) | Apparent permeability after test $K_2$ g/(cm/torr·sec | $\frac{K-K_1}{K} = \frac{A-A_1}{A}$ | Cesium flow $j(ma/cm^2)$ at 300°C $A_1 = .157\ cm^2$ |
|---|---|---|---|---|---|
| SP1 | $1.42\times10^{-6}$ | $0.37\times10^{-6}$ | $0.473\times10^{-6}$ | .74 | 3.30 |
| SP2 | 0.92 | 0.493 | 0.632 | .462 | 4.47 |
| SP3 | 1.17 | 0.628 | 0.624 | .464 | 3.78 |
| SP4 | 1.17 | 0.553 | 0.488 | .528 | 1.0 |
| SP5 | 0.92 | 1.21 | -- | (-.315)? | -- |
| Average | 1.12 | .650 | .554 | .548 | |

FIG. 6 IONIZER CROSS-SECTION AND PATTERN OF BRAZE PENETRATION

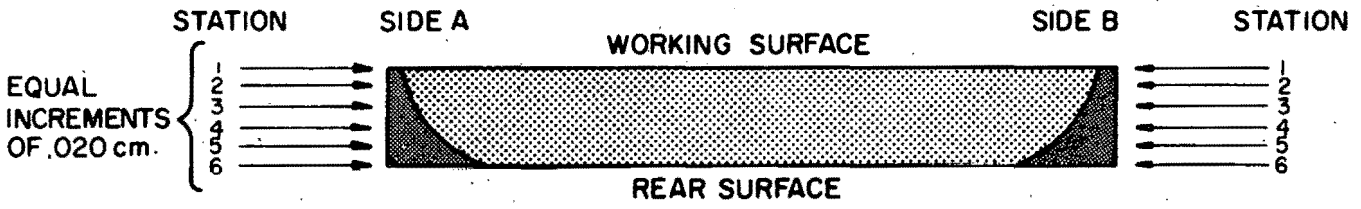


TABLE II

MICROSCOPIC MEASUREMENT DATA OF BRAZE PENETRATION INTO SPHERICAL POWDER IONIZER SP2

| Station No. | Measured Penetration, cm Side A | Side B | Avg. | True Pen. .883xAvg. | True Pen. x 2 | True Dia. -2x True Pen. | Porous Area, $cm^2$ |
|---|---|---|---|---|---|---|---|
| 1* | .0204 | .0151 | .0177 | .0156 | .0312 | .447 | .1569 |
| 2 | .0250 | .0154 | .0202 | .0178 | .0356 | .442 | .1534 |
| 3 | .0235 | .0493 | .0364 | .0321 | .0642 | .414 | .1346 |
| 4 | .0589 | .0643 | .0616 | .0544 | .1088 | .369 | .1069 |
| 5 | .0723 | .0710 | .0716 | .0632 | .1264 | .352 | .0973 |
| 6** | .0860 | .0741 | .0800 | .0706 | .1412 | .337 | .0892 |

*working surface
**rear surface

Apparent section-diameter of button = 0.422 cm

True diameter of button (measured with micrometer) = 0.478 cm

Correction factor (due to off-center sectioning) = 0.422/0.478 = .883

Initial area of unmounted button = .1791 $cm^2$

A different type of braze infiltration is seen for the wire bundle ionizer in Fig. 7 which in general have much larger pore sizes. The apparent nitrogen permeability is compared for all ionizers in Table III. The apparent nitrogen permeability of the average SP ionizer is 2 - 3 times that of the average SW ionizer. The WB ionizers are about 10 times more permeable.

The commercial sintered tungsten ionizers (designated by the symbol SW) were selected from a large number of buttons to have a range of permeabilities convenient for a reasonable cesium reservoir temperature and a fine and stable pore structure. The average spherical powder ionizers (designated by the symbol SP) and the wire bundle ionizers (designated by WB) were made by H. Todd and M. LaChance of Electro-Optical Systems, Inc. under NASA Contract.

## 6. CESIUM PERMEABILITY AND ITS CHANGE WITH TEMPERATURE

A measure of cesium conductance can be obtained in two ways: 1) by using the cesium atom probe and 2) by measuring cesium ion current. The neutral probe current was measured for two SW and two WB ionizers used for the study of angular distribution of the cesium effusion pattern. The probe current on the ionizer axis is assumed to be directly proportional to the total cesium flow in particles per second. Curves in Fig. 8 show that the cesium conductance of WB ionizers was about 50 x that of SW ionizers. Each group had a spread of factors up to 10.

The second type of cesium conductance estimate is the ion current density in Fig. 9 which does not include neutrals. For SW and SP ionizers the actual cesium conductance in equivalent $ma/cm^2$ was 1-15% higher and for WB about 5-50%. Note also that higher current densities required higher ionizer temperatures. The cesium conductance is slightly dependent upon the ionizer temperature as seen in Fig. 10. The ionizer was not held at constant temperature in Fig. 9. The ion current measurement gives the value of cesium conductance which is converted to an apparent cesium permeability

TABLE III

APPARENT NITROGEN PERMEABILITY OF MOUNTED IONIZERS

| Ionizer Identity | K, $\frac{10^{-6}\ gm}{cm \cdot torr \cdot sec}$ |
|---|---|
| Commercial Sintered | |
| SW1 | .078 |
| SW2 | .122 |
| SW3 | .226 |
| SW4 | .186 |
| SW5 | .257 |
| SW6 | .285 |
| SW7 | .570 |
| Average | 0.246 |
| Spherical Powder | |
| SP1 | .37 |
| SP2 | .493 |
| SP3 | .628 |
| SP4 | .553 |
| SP5 | 1.21 |
| Average | .650 |
| Wire Bundle, 12 μ | |
| WB1 | 1.41 |
| WB2 | 1.37 |
| WB3 | 2.90 |
| WB4 | 3.34 |
| WB5 | -- |
| Average | 2.25 |
| Wire Bundle, 6μ | |
| WB6 | 2.58 |

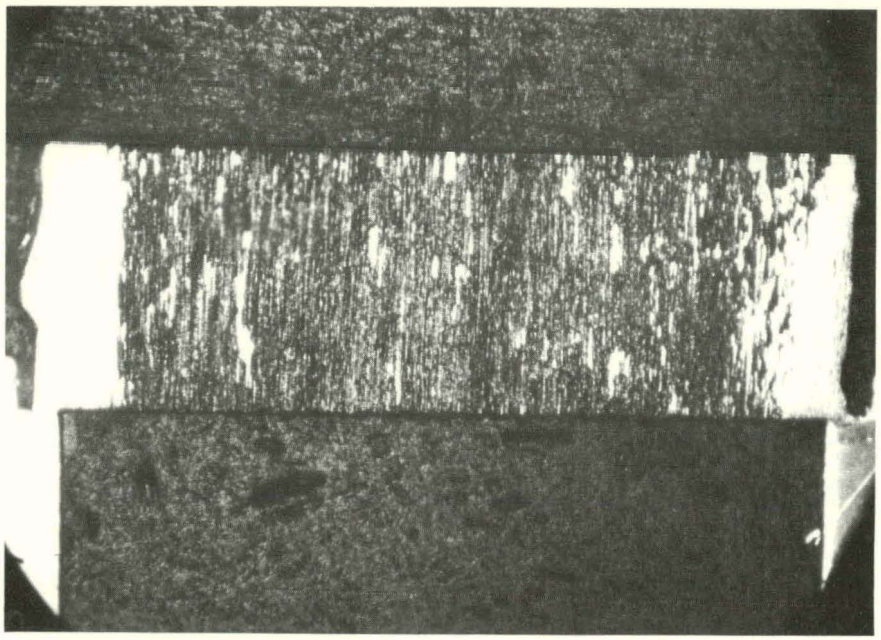

FIG. 7 CROSS SECTION OF A 12 MICRON WIRE BUNDLE IONIZER SHOWING BRAZE INFLATION 22X MAGNIFICATION

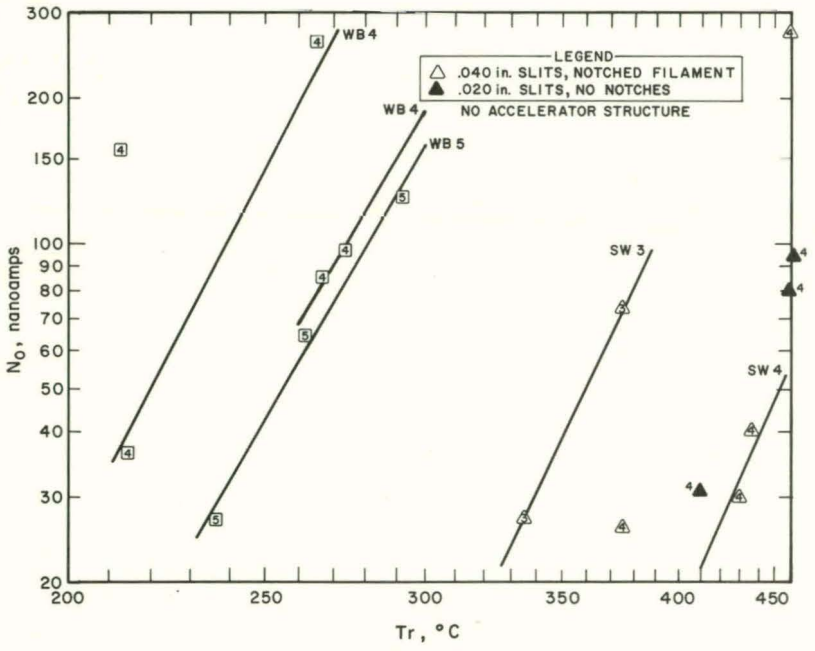


FIG. 8

TOTAL CESIUM FLOW MEASURED BY NEUTRAL DETECTOR WITHIN $\pm$ 5° OF THE ANGULAR DISTRIBUTION PEAK

No accelerator structure.

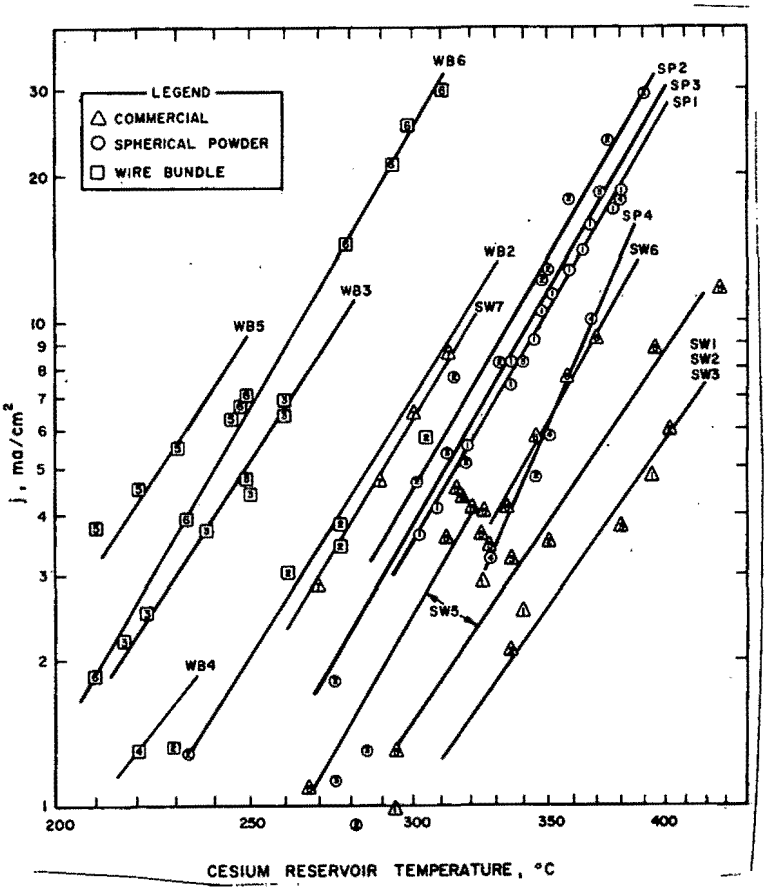


FIG. 9

CESIUM CURRENT DENSITY AS A CESIUM PERMEABILITY INDICATOR FOR THE VARIOUS TUNGSTEN IONIZERS

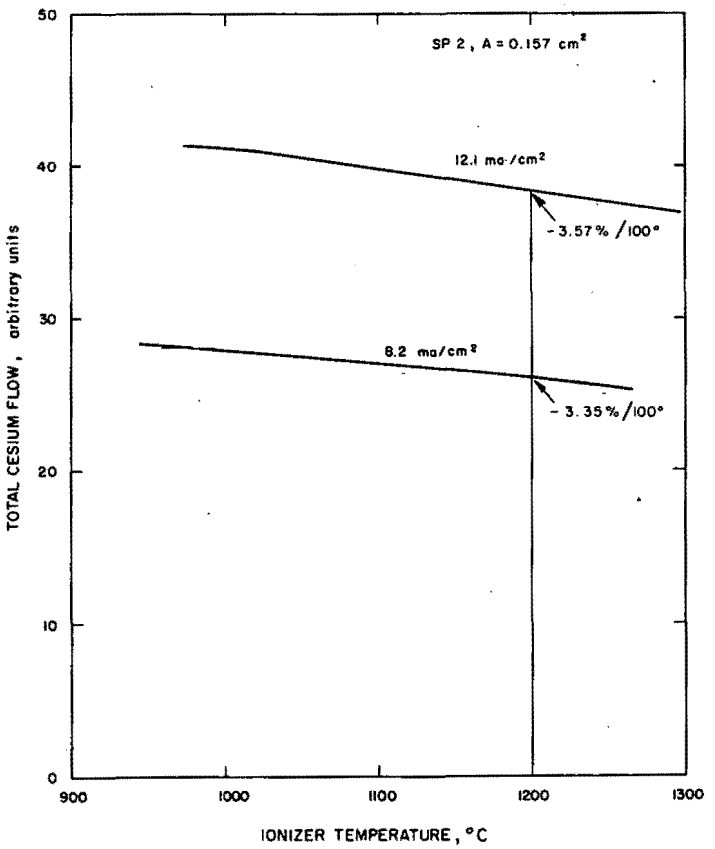


FIG. 10

CHANGE OF CESIUM PERMEABILITY WITH IONIZER TEMPERATURE AT HIGH SURFACE COVERAGE

measurement by normalizing to equal areas for each of the ionizer groups. The best estimates of the active areas are .157 $cm^2$ for SW and SP ionizers, except for SW1 which was .220 $cm^2$, and .141 $cm^2$ for WB ionizers. The results in Fig. 9 are similar to those in Fig. 8. The SP ionizers have apparent cesium permeabilities 3 times higher and the WB about 10 to 20 times higher than the SW ionizers.

There is not enough data to statistically compare nitrogen and cesium permeabilities and to speculate about the nature of the transport mechanism. The change of cesium conductance with temperature can be measured with the atom probe assuming that the angular distribution does not change with ionizer temperature. Figure 10 shows the decrease of ionizer permeability with temperature as measured by the neutral probe on the geometric axis. In this case there is no voltage applied, no surface ionization and there is a high surface coverage. The equivalent ion current density indicated for each curve gives the average ion current which would be generated at this flow rate (or cesium temperature) with 100% ionization. The temperature coefficients of conductance shown were computed at $T_e = 1200^{\circ}C$. Figure 11 shows the percent change of cesium flow as measured by a neutral probe for a wire bundle. This particular ionizer exhibited a hysteresis which somewhat depended upon the rate at which the temperature was varied. This hysteresis was exactly opposite to what one would expect if there was some storage effect on the surface or inside the ionizer. Since the WB ionizers are very permeable the flow drifted slowly as heat transfer from the ionizer heated up the cesium reservoir. The curves were corrected for this slow drift. The hysteresis effect had a much smaller time constant.

## 7. ACTIVE IONIZER AREA AND ION CURRENT DENSITY MEASUREMENT

Measurement of the active ion emission area is needed for the calculation of ion current density. The active area can be estimated:

a) by microscopic observation of ionizer surface for a color change around the edges.

b) by comparison of nitrogen conductance before and after brazing into the holder.

c) by obtaining a sputtering pattern in a parallel plane arrangement.

d) by low magnification ion microscopy.

e) by a photomicrograph of the ionizer cross section, which destroys the ionizer.

The first method is the simplest, but is not very reliable. The second method gives the relation between true and apparent nitrogen permeability, but does not give an accurate measure of active area as discussed in the previous section.

A more reliable method is the measurement of active emission area by the sputtering pattern. The ionizer is placed into a plane-parallel diode arrangement with a copper cathode and a gap of about .175 inches. Emission-limited operation is maintained to assure parallel ion trajectories. This produces a well defined sputtered area which is assumed to be equal to the active ion emission area. The sputtering pattern area for SW7 was .155 $cm^2$, compared to .157 $cm^2$ measured by metallographic cross section for SP2. Based on these two measurements active areas for all SW and SP ionizers were assumed to be 0.157 $cm^2$.

For the wire bundle the surface closure measured from Fig. 7 was 15.2% and the penetration pattern was different. The .141 $cm^2$ area used for most 12 micron wire bundles was obtained by method a). For the fine wire bundle, the sputtering pattern gave an area of 0.114 $cm^2$ or a 23% closure.

The measurement of ion current is made at a collector and involves the following assumptions:

1) The entire beam emerging from the engine is collected. This is checked by a visual observation of the target luminescence area,

usually from 1 to 3 inches in diameter. The collector diameter is 10 inches. It can also be checked by visual observation of the beam angle in argon. A third check is provided by the I-V characteristic. When some of the beam misses the target, this fraction usually depends upon the voltage and produces an irregular I-V curve.

2) There is no secondary electron-emission current away from the collector. This is checked by increasing the secondary electron-suppressor voltage until the collector current no longer decreases.

3) There is negligible interception of the emitted ions by the accelerating structure. Ion interception at the accel electrode is small but measurable. Measurements are complicated by electron currents.

The active surface area measurement includes the following additional assumptions:

a) Emission is from the apparent geometrical area, without regard to the ratio of pore area/closed area or to any true solid area dependent on roughness and grain structure of the surface.

b) There is no emission from the brazed area or the holder. Most of the above factors, would tend to increase the current density, hence our measurements reflect a conservative value.

A typical current-voltage characteristic is shown in Fig. 12. The ratio of accelerator ($V_-$) to ionizer ($V_+$) voltage is kept constant and equal to 2. This is equal to an accel-decel ratio $(V_- + V_+)/V_+$ of 3. The accelerator perveance for this curve is 30 nanopervs or 191 nanopervs/$cm^2$, using for the area the active area of 0.157 $cm^2$ corresponding to a braze infiltration of 12 percent.

## 8. THE ANGULAR DISTRIBUTION OF ATOMS, NEUTRALS, IONS AND NEUTRAL FRACTION

An important ionizer performance figure of merit is the neutral fraction. The neutral fraction is defined as the ratio of neutrals to the total efflux of cesium ions and neutrals. The term "neutrals" in this report will be used specifically for the case where the

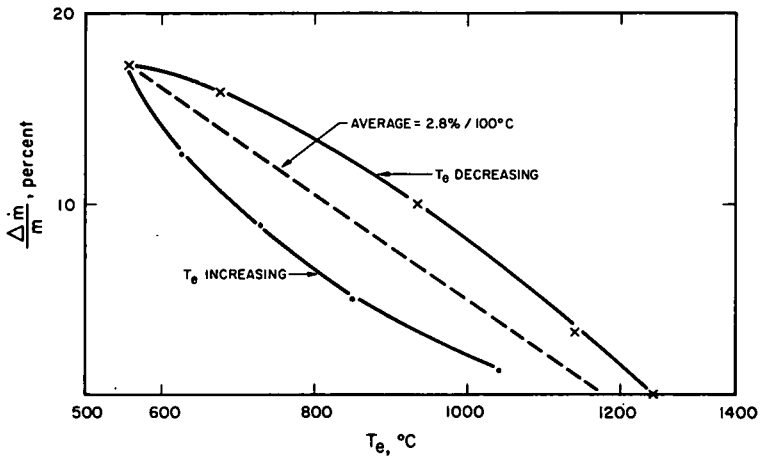


FIG. 11 PERCENT CHANGE OF CESIUM FLOW VS IONIZER TEMPERATURE FOR COMPRESSED WIRE BUNDLE NO. 4

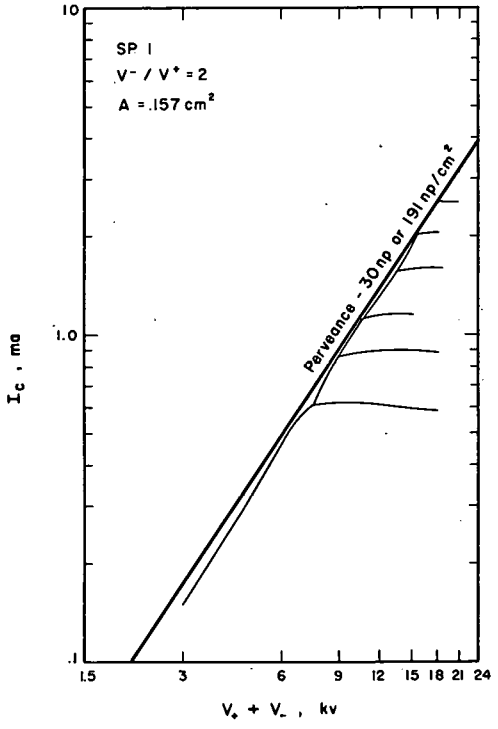


FIG. 12

TYPICAL CURRENT VOLTAGE CHARACTERISTICS FOR A SPHERICAL POWDER IONIZER

accelerating voltage is applied and an ion beam is being extracted. The term "atoms" will be used for the case where no accelerating voltage is applied and the entire efflux is atoms.

Since, with the use of a probe, a small portion of the neutral fraction rather than the total is measured, one must ascertain whether the neutral fraction is independent of the angle. For this reason the angular distributions of neutrals, atoms and neutral fractions were studied in detail. In some of the measurements the slit widths were .040 inches with a notched tungsten filament. In some of the latter experiments the slit widths were reduced to 0.020 inches and the notches eliminated to reduce the chance of systematic angular error.

The angular distribution of cesium atoms evaporating from a commercial sintered porous tungsten ionizer without any accelerating structure is shown in Fig. 13 as a function of the flow rate. This distribution is very nearly cosine. It is typical for most measurements of this type and it was independent of the cesium flow rate or of the ionizer temperature. The angular distribution of cesium atoms evaporating from a wire bundle showed a very definite peak and it deviated more from the cosine law depending upon the nature of the mechanical surface treatment. Figure 14, for example, shows a highly peaked pattern obtained with an etched wire bundle. The etching has opened up the pores. Distributions for some of the other wire bundle ionizers were not as highly peaked because their surface pore openings were reduced by mechanical abrading or by compression of the button. This definitely suggests that the atoms evaporating from a wire bundle come to some degree from within the pores. A shielding effect of the electrode on the distribution of atoms is shown in Fig. 15 or from comparison with the curve for the case without electrodes. A complete study of the angular distributions of ions, atoms, neutrals and neutral fraction through electrodes for a wire bundle, WB5, is shown in Fig. 16. These curves illustrate

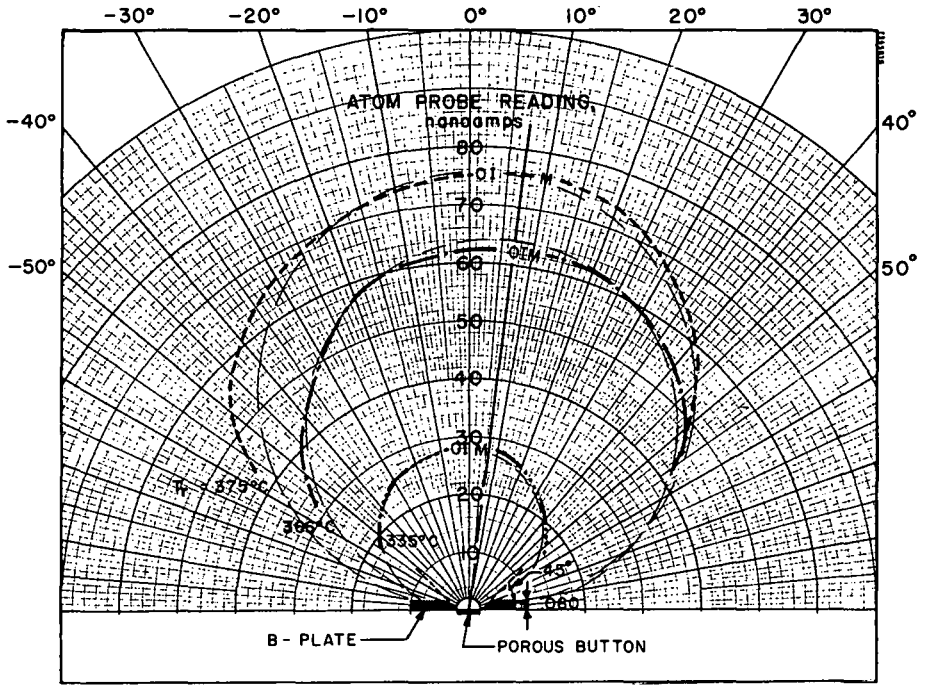


FIG. 13

ANGULAR DISTRIBUTION OF CESIUM ATOMS EVAPORATING FROM A COMMERCIAL SINTERED POROUS TUNGSTEN IONIZER AS A FUNCTION OF CESIUM FLOW RATE SW 3, $T_e$ = 1200°C, B-plate only, probe has .040" slits and a noted filament.

M - Line of maximum

I - Center line of averages

O - Line through center of circles

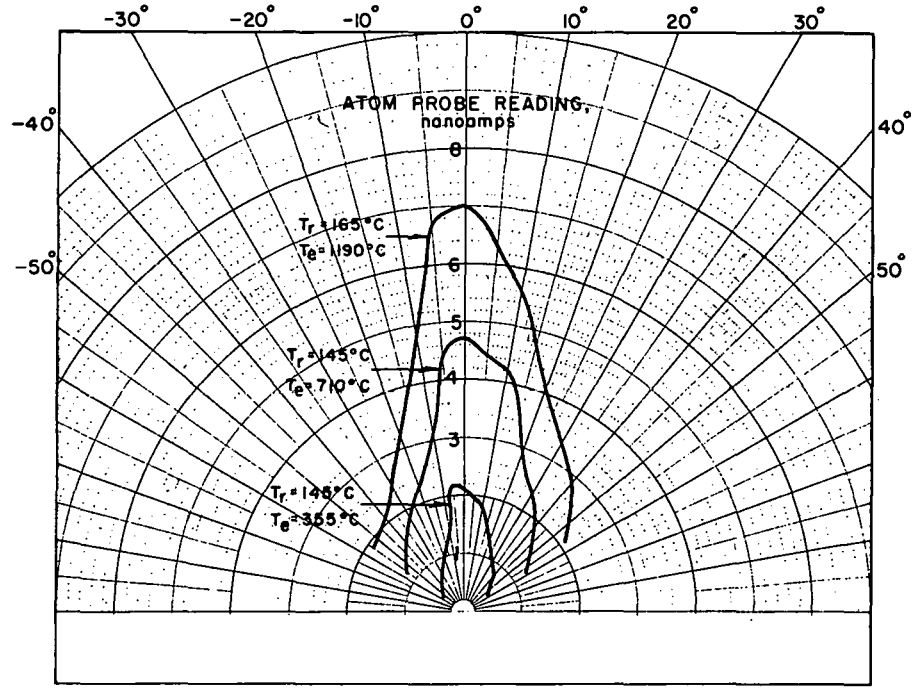


FIG. 14

ANGULAR DISTRIBUTION OF CESIUM ATOMS AS A FUNCTION OF IONIZER TEMPERATURE ETCHED WB 5, .020" slits, unnotched filament

that the neutral fraction cannot be measured with this probe inside of the ion beam which is about $18^{o}$ wide. The signal due to ions is considerably larger than due to atoms or neutrals. The neutral detector can be used for a study of ion beam profiles illustrated in Fig. 17 on a rectangular plot. These curves illustrate the ion beam expansion from a total included angle of $8^{o}$ to about $30^{o}$ as the current density is increased from about 3 to about 12 $ma/cm^2$ even though the voltage is also increased.

To measure the angular dependence of the neutral fraction either a single screen accelerating electrode was used as shown in Fig. 18 or a set of slotted accel-decel electrodes were used as in Fig. 19. In both cases the neutral fraction appeared reasonably constant within an angle of about $20^{o}$ just outside of the ion beam and before the signal strength falls off to a very low value. Most of the checks of the constancy of neutral fraction with angle were done in the presence of the regular electrodes. A set of curves for a wire bundle including neutral fraction was already shown in Fig. 16. A similar set of curves for a commercial sintered tungsten ionizer is shown in Fig. 20. A set of neutral fraction curves for a large range of current densities is shown in Fig. 21. As seen from these curves there is always a range of angles just outside of the beam, and before the signal strength declines into the noise level, in which the neutral fraction is relatively constant. Observe also that the range changes with the current density. At higher current densities the beam expands more and the neutral eye must be located at a larger angle or made insensitive to the presence of the energetic ions. The $15^{o}$ position of the neutral detector appears to be adequate for current densities of up to about 15 $ma/cm^2$.

## 9. ION CURRENT DENSITY, NEUTRAL FRACTION AND CRITICAL TEMPERATURES

The most popular measurement in surface ionization is the ion current density as a function of ionizer temperature for various cesium flow rates. A set of typical curves for solid tungsten as

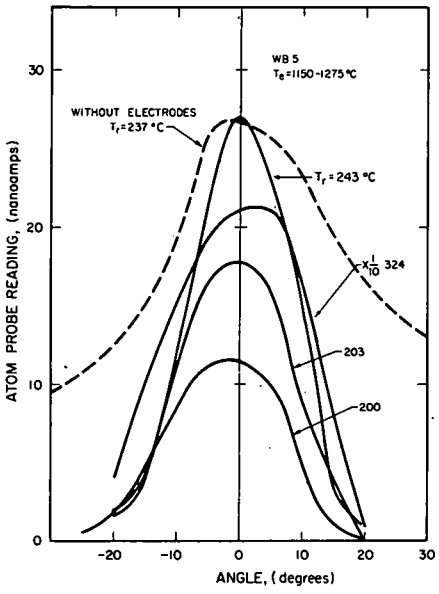


FIG. 15

ANGULAR DISTRIBUTION OF ATOMS THROUGH ELECTRODES

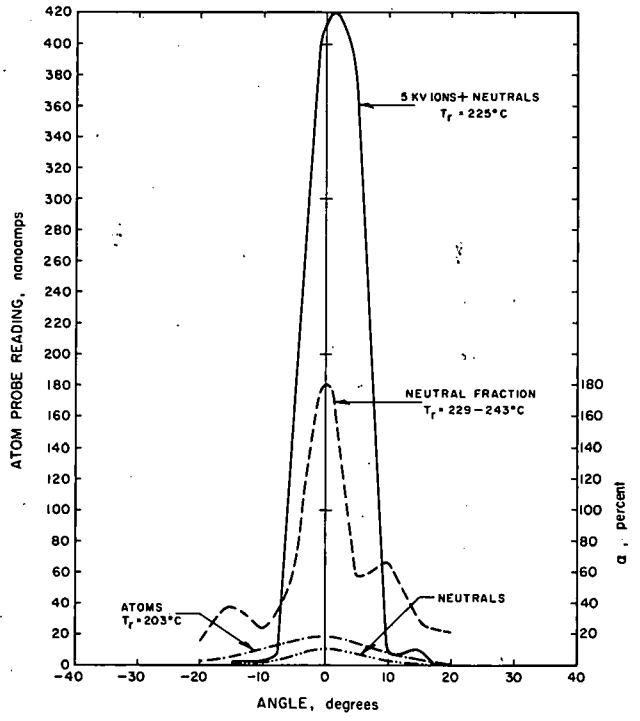


FIG. 16

ANGULAR DISTRIBUTION OF IONS, ATOMS, NEUTRALS AND NEUTRAL FRACTION THROUGH ELECTRODES WB 5

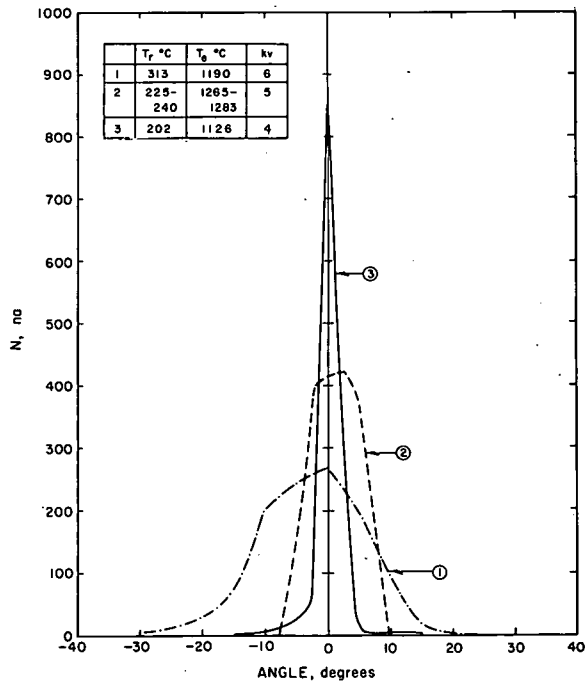


FIG. 17

ION BEAM PROFILES FOR A WIRE BUNDLE IONIZER

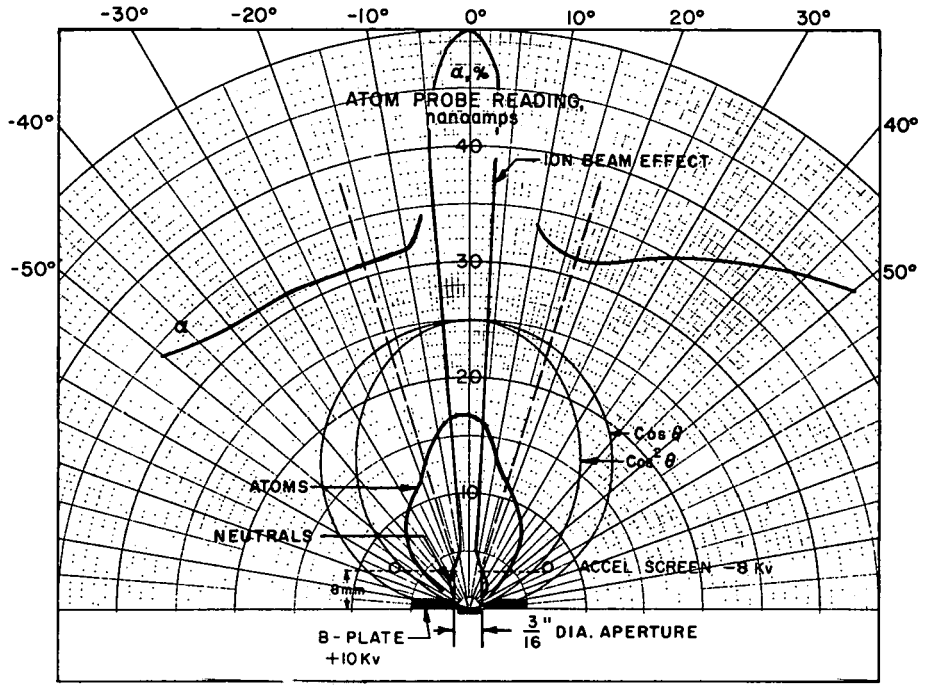


FIG. 18

ANGULAR DISTRIBUTION OF ATOMS, NEUTRALS AND NEUTRAL FRACTION FOR COMMERCIAL TUNGSTEN IONIZER SW 3 USING A WIRE SCREEN ACCELERATOR ELECTRODE

$T_e$ = 1020°C, $T_r$ = 335°C, j = 2.5 ma/cm$^2$; 20 mesh, .016" copper wire screen, 46.2% open; atom probe had .04 " slits and notched filament.

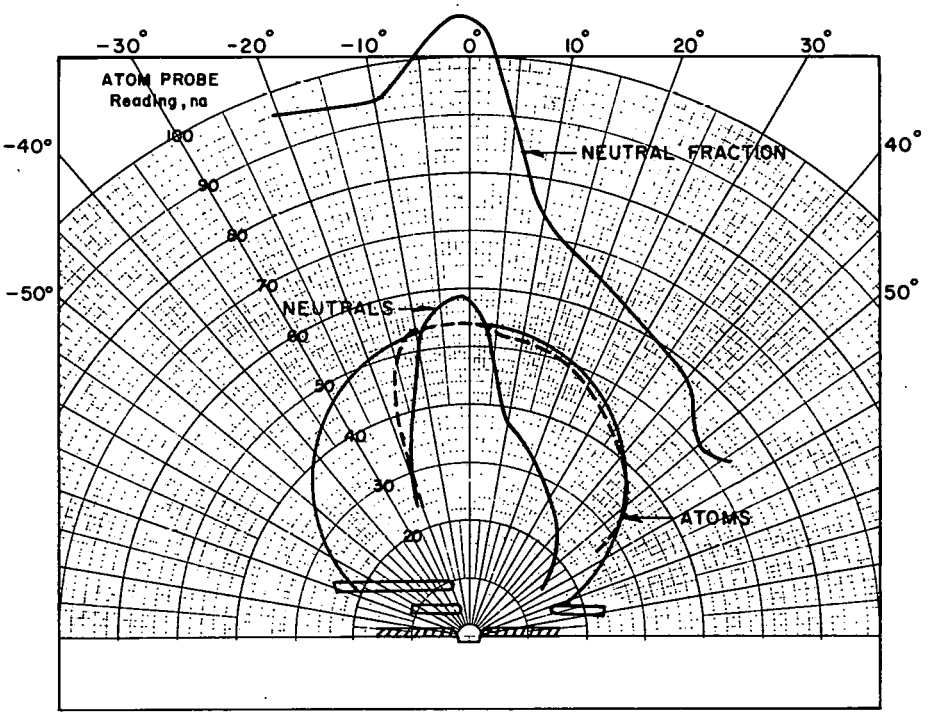


FIG. 19

ATOM, NEUTRAL AND NEUTRAL FRACTION DISTRIBUTION FOR WIRE BUNDLE IONIZER WB 4 USING SLOTTED ELECTRODES

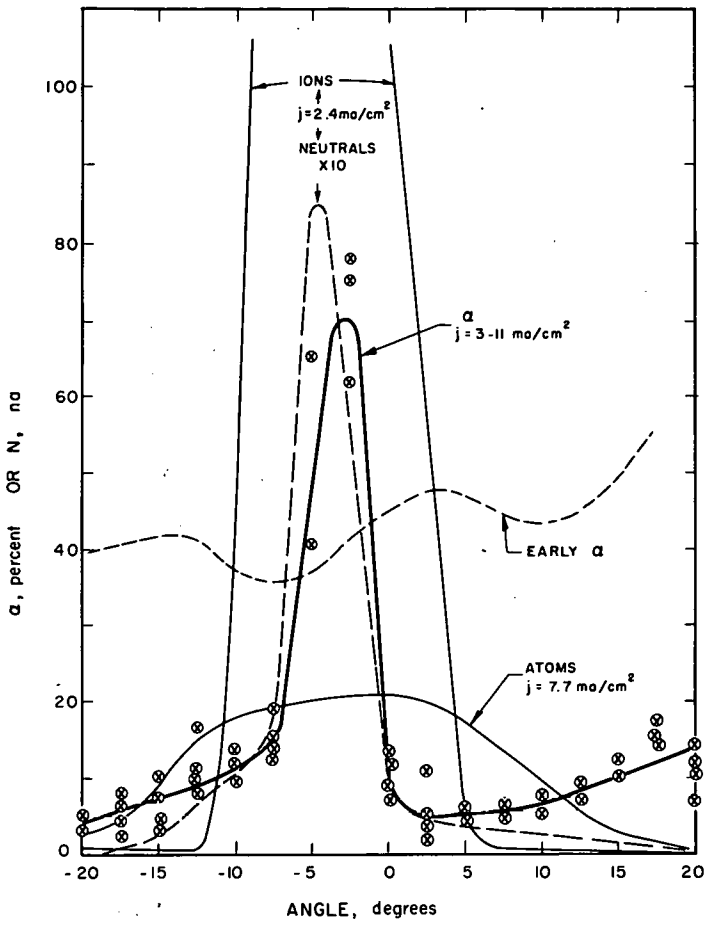


FIG. 20

ANGULAR DISTRIBUTION OF NEUTRAL FRACTION, NEUTRALS, ATOMS AND IONS FOR SW 5

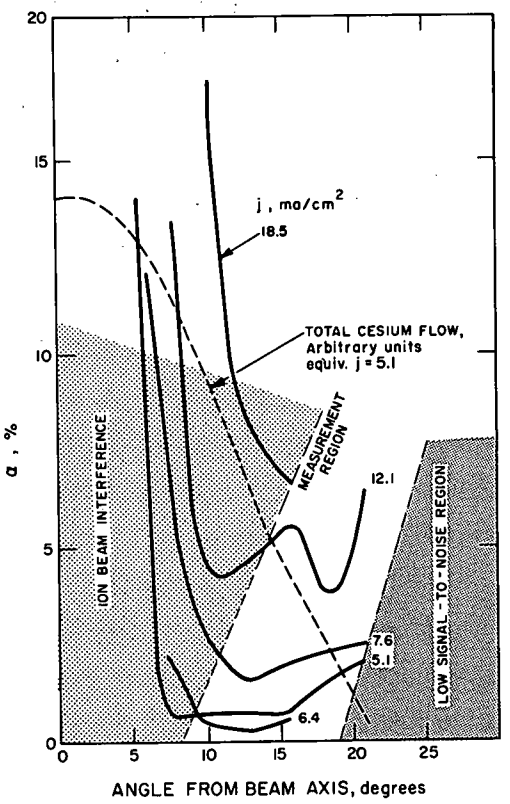


FIG. 21

ANGULAR DEPENDENCE OF NEUTRAL FRACTION AND TOTAL CESIUM FLOW (AS NEUTRALS) FOR SPHERICAL POWDER IONIZER SP 2

measured by Langmuir (33TL) is shown in Fig. 22 to define the various regions of operation. These data are usually taken with decreasing temperatures. At high temperature the cesium coverage is low and for high work function surfaces the ionization is so nearly 100% that it appears essentially constant. At a certain temperature called the critical temperature the ion current discontinuously drops by more than a decade as the surface becomes covered with cesium. In the high coverage region the decline is exponential.

For the porous ionizer the typical current-temperature curve is more like that in Fig. 23. The low coverage region is most likely no longer constant because of a change in ionization efficiency and ionizer permeability with ionizer temperature. Instead of a discontinuity there is a transition region characterized by a large change in the slope. There are sometimes two "critical temperatures" - one, $T_{CI}$, defined as the temperature at which the ion current has declined by 5%, the other - $T_{C\alpha}$ defined as the temperature corresponding to minimum neutral fraction.

A typical set of selected data for SP1 ionizer illustrates the various definitions and graphing techniques in Fig. 24. The current density $j_c$ is based upon an area of 0.179 $cm^2$ and was not corrected for 12% braze closure. Hence, the true ion-current density is 12% higher. All curves were taken with decreasing ionizer temperatures and the $T_{CI}$ points are the lower critical temperatures which may be below the minimum operating temperature for the ionizer. The transition with increasing temperatures can occur at a higher temperature (about 10 - 30°) called the upper critical temperature. The log j vs 1/T plots are used because, for solid tungsten, the $T_{CI}$ points fall on a line marked $T_{CI}$-Langmuir. The $T_r$ parameter indicated is the temperature of the cesium reservoir in °C.

Simultaneous with the ion current, the neutral fraction is measured and the corresponding points are plotted in Fig. 24. Sometimes the temperature $T_{C\alpha}$ corresponding to minimum neutral fraction

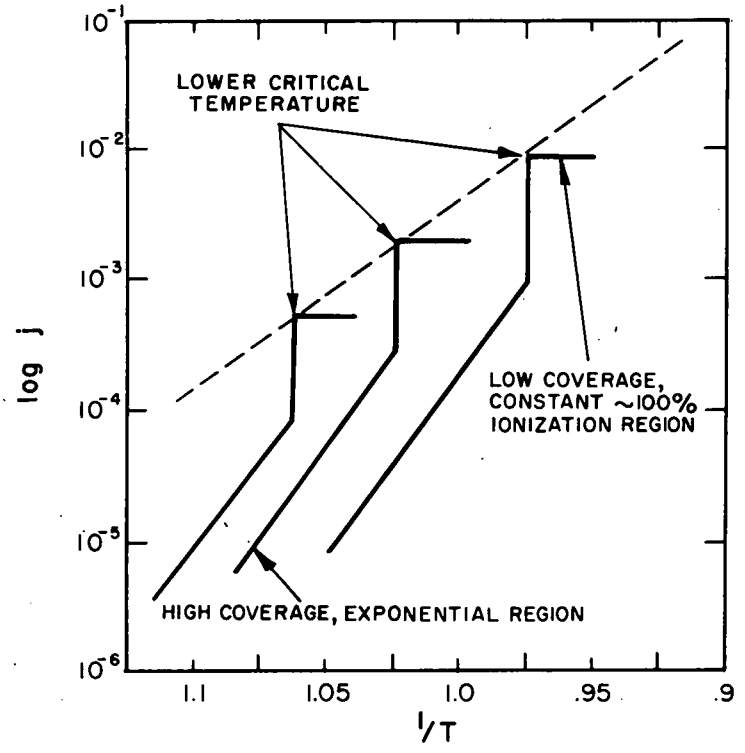


FIG. 22

DEFINITIONS OF SURFACE IONIZATION REGIONS FOR ION CURRENT-IONIZER TEMPERATURE CURVES FOR SOLID TUNGSTEN (from 33TL)

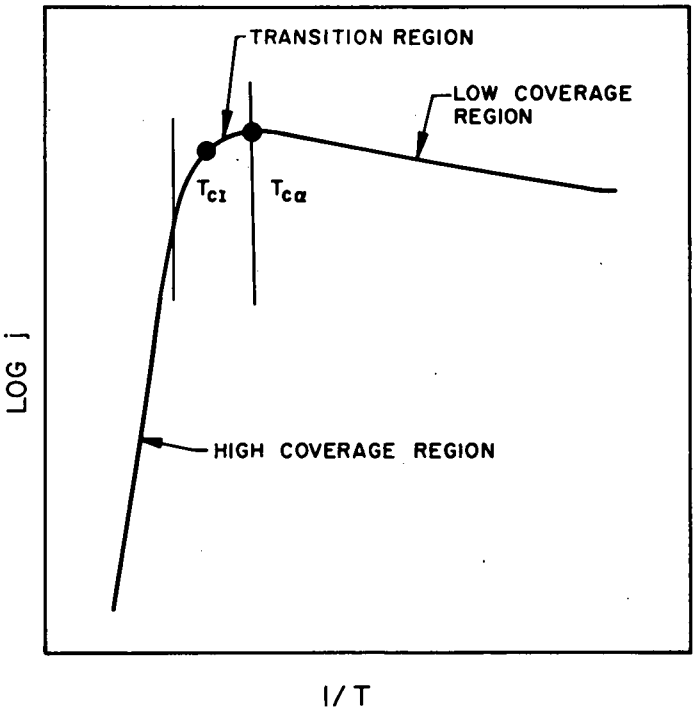


FIG. 23

DEFINITIONS OF SURFACE IONIZATION REGIONS FOR CESIUM ON TYPICAL POROUS TUNGSTEN IONIZERS

the SP1 ionizer should be operated at least 100°C hotter than the $T_{CI}$ line. The $T_{CI}$ points in the $j_c$ versus 1/T plot coincide closely to the $\alpha_m$ = +5 percent line in the $\alpha$ versus 1/T plot. If 6 - 8 percent neutral fractions cannot be tolerated, the ionizer must be operated at a temperature above the $T_{CI}$ line. However, one does not have to go to $\alpha_m$. As the lines 1.2 $\alpha_m$, 1.5 $\alpha_m$, and 2 $\alpha_m$ indicate, the change of $\alpha$ near the minimum is very slow. A 30° increase in temperature decreases $\alpha$ by more than 50 percent. Optimum ionizer operation is therefore close to the $T_{CI}$ line and between $T_{CI}$ and $T_{C\alpha}$ in Fig. 24a, corresponding to about the 1.5 $\alpha_m$ line in Fig. 24b.

Figures 25a and 25b contain a summary of all critical temperature points for SP1 ionizer obtained from points on all curves similar to those in Figs. 24a and 24b. The number with each point indicates the day and order in which the curves were taken. For example, 32 was taken during the third day of testing and it is the second curve. Such graphical summaries of critical points for each ionizer with the order identified show the time trends, especially during the initial period of ionizer conditioning. As seen by comparison with Fig. 24a the critical temperature $T_{CI}$ and $T_{C\alpha}$ has decreased by about 100° from the first day to the third day. Figure 25b summarizes all neutral fraction values $\alpha_{CI}$ corresponding to $T_{CI}$ and $\alpha_m$ corresponding to $T_{C\alpha}$, showing the time measurements. The $\alpha_m$ values for this ionizer are much lower than the $\alpha_{CI}$. The $\alpha_{CI}$ is very nearly equal to $\alpha_m$ + 5. For this ionizer, $\alpha$ curves on the first day showed no definite minimum up to 1300°C and their slopes were lower.

To establish the performance of a given porous structure several ionizers of the same structure must be tested. The current and neutral fraction versus critical temperature points of four spherical powder ionizers are shown in Fig. 26. Neglecting the points measured during the conditioning period, the current versus

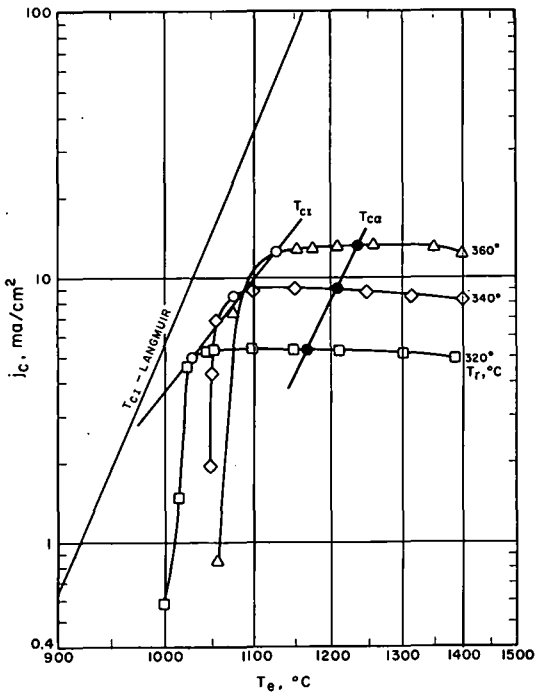


FIG. 24a LOG $j_c$ VS $1/T_e$

CURVES DEFINING TWO "CRITICAL TEMPERATURE" POINTS FOR SP 1 IONIZER

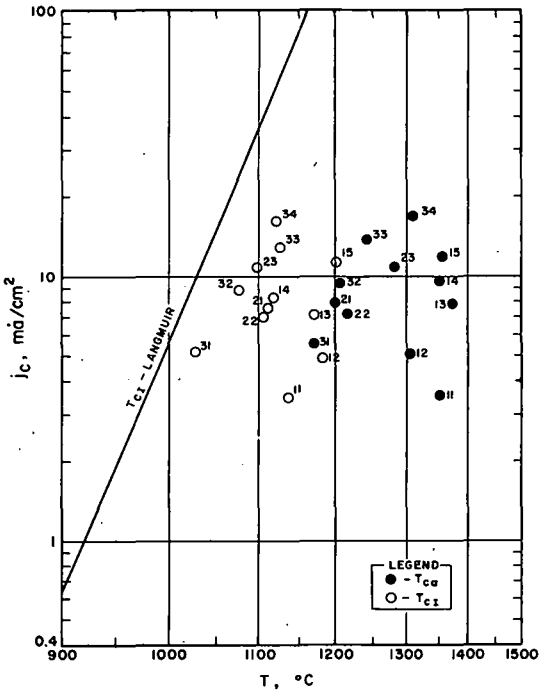


FIG. 25a LOG $j_c$ VS 1/T - SUMMARY OF ALL CRITICAL POINTS FOR SP 1 IONIZER

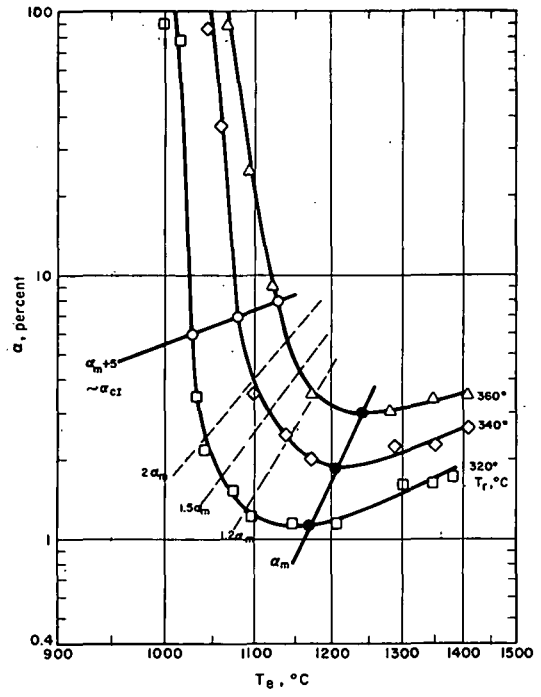


FIG. 24b LOG $\alpha$ VS $1/T_e$ CURVES

SHOWING NEUTRAL FRACTION CORRESPONDING TO CURVES IN FIG. 24a

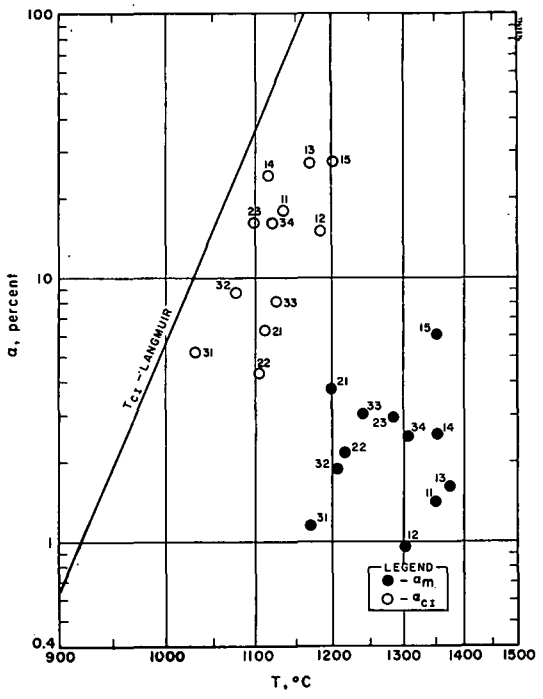


FIG. 25b LOG $\alpha$ VS 1/T - SUMMARY OF ALL CRITICAL POINTS FOR SP 1 IONIZER

critical temperature points are in a band marked $T_{CI}$-SP. This band is about 75°K wide and starts about 25°K above the Langmuir line. The neutral fraction critical temperature points fall in a similar band marked $T_{C\alpha}$-SP which is 125°K wide and starts about 150°K above the Langmuir line.

A similar summary of $T_{CI}$ points for commercial sintered tungsten ionizers, given in Fig. 27 shows a larger spread. For most SW ionizers the $T_{C\alpha}$ points were identical with $T_{CI}$.

A typical set of ion current density and neutral fraction curves for a 12 micron wire bundle ionizer with critical temperature points is shown in Fig. 28. Note the much higher neutral fractions and the coincidence of most $T_{CI}$ and $T_{C\alpha}$ points except at low $\alpha$ values.

The fine wire bundle ionizer $\alpha$ curves in Fig. 29 showed much more pronounced minima especially at low flow rates. Because of ionizer to reservoir heat flow the reservoir temperature depended upon the ionizer temperature. The nature of the $\alpha$ curves changed with ionizer conditioning. Numbers with each curve again indicate their order

The log $\alpha$ vs $T_e$ graphs (Fig. 24b) are most useful in establishing the neutral fraction critical temperature $T_{C\alpha}$ and the values of $\alpha_{CI}$ at the ionizer critical temperature. To compare the neutral fractions of various ionizers and structures, a plot of $\alpha$ vs j is used. Figure 30 shows the minimum neutral fraction of several ionizers for the various porous tungsten structures. Some of the spread for each ionizer is caused by the time dependence illustrated in Fig. 31. Note the large reduction during the initial conditioning and the smaller change on each successive day. The commercial porous tungsten ionizers, except for SW5, and the spherical powder ionizers generally have neutral fractions ranging from a fraction of percent to 10 percent at 30 ma/cm$^2$. This is higher than given by the Langmuir data for solid tungsten. The large neutral fractions of the 12 micron wire bundle ionizers are probably due to the opening of the pores

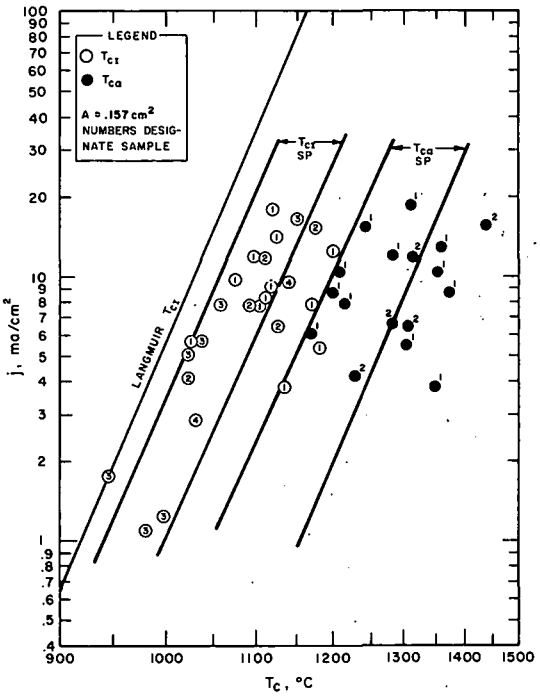


FIG. 26

SUMMARY OF CURRENT AND NEUTRAL FRACTION CRITICAL TEMPERATURE POINTS FOR FOUR SPHERICAL POWDER IONIZERS

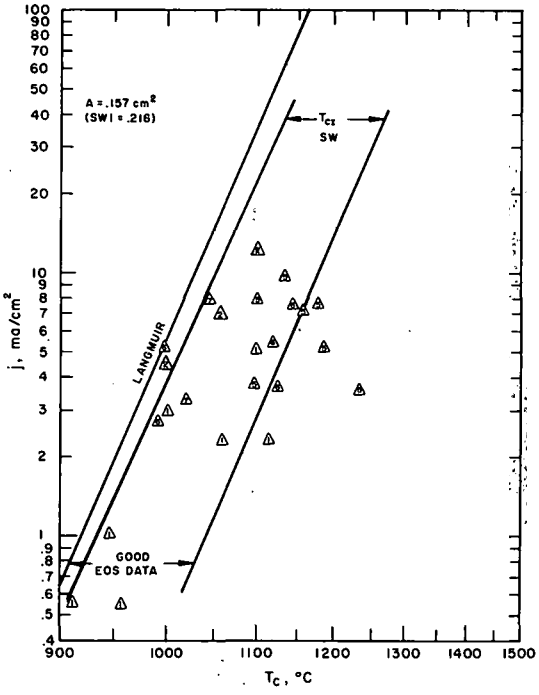


FIG. 27

SUMMARY OF $T_{cI}$ POINTS FOR FIVE COMMERCIAL SINTERED TUNGSTEN IONIZERS

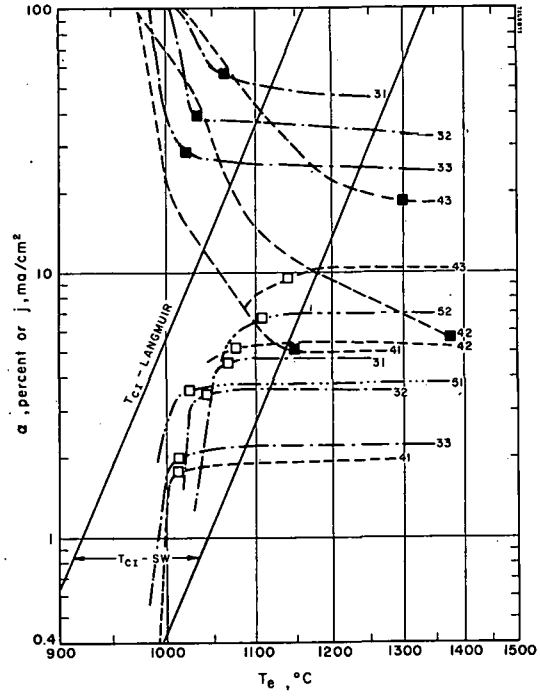


FIG. 28

ION CURRENT AND NEUTRAL FRACTION VS IONIZER TEMPERATURE FOR COARSE WIRE BUNDLE NO. 3

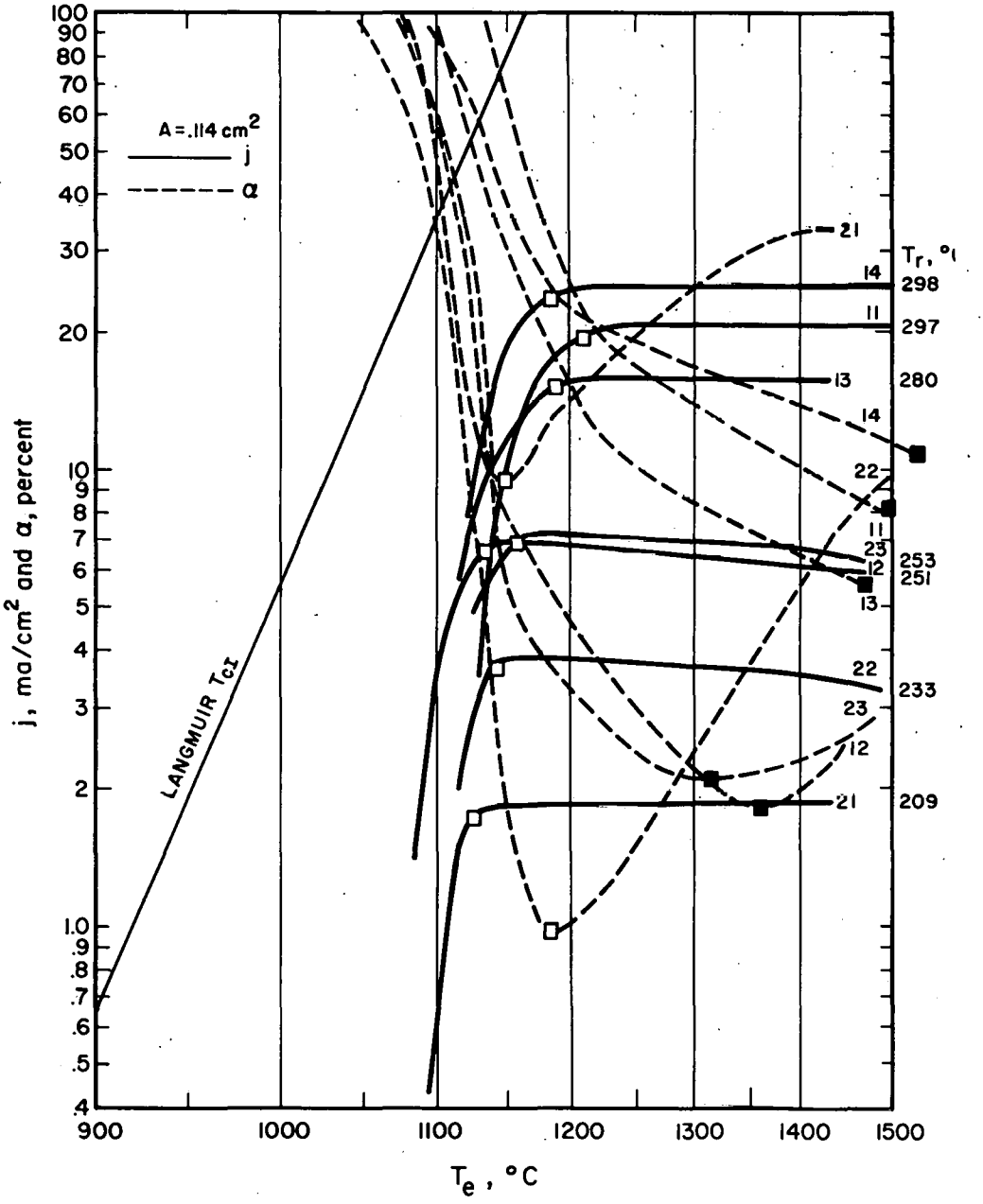


FIG. 29 ION CURRENT AND NEUTRAL FRACTION VS IONIZER TEMPERATURE FOR FINE WIRE BUNDLE NO. 6

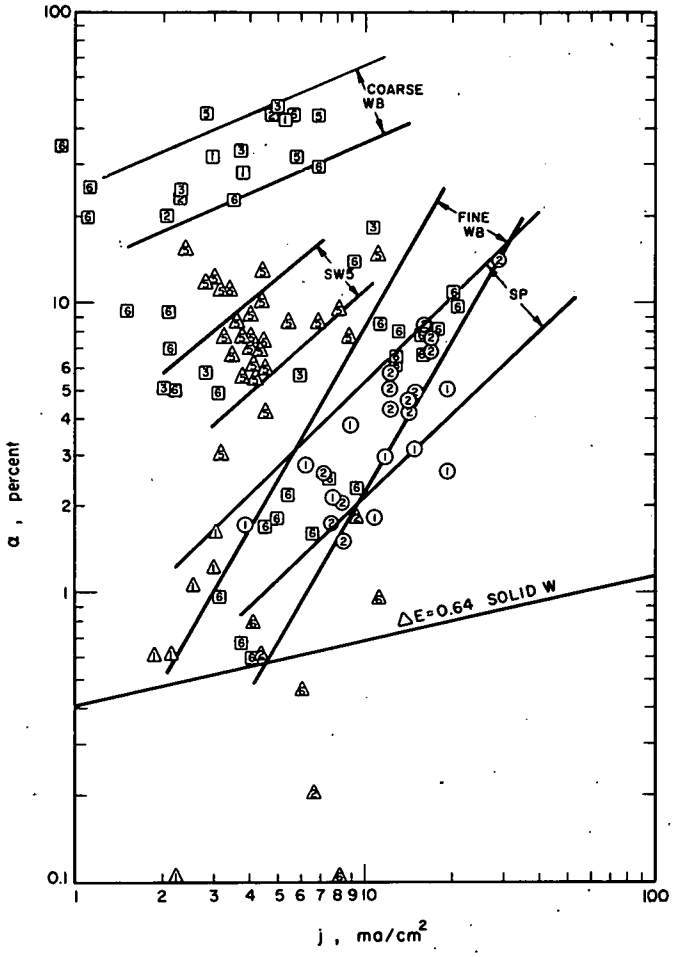


FIG. 30

NEUTRAL FRACTIONS FOR VARIOUS POROUS TUNGSTEN STRUCTURES

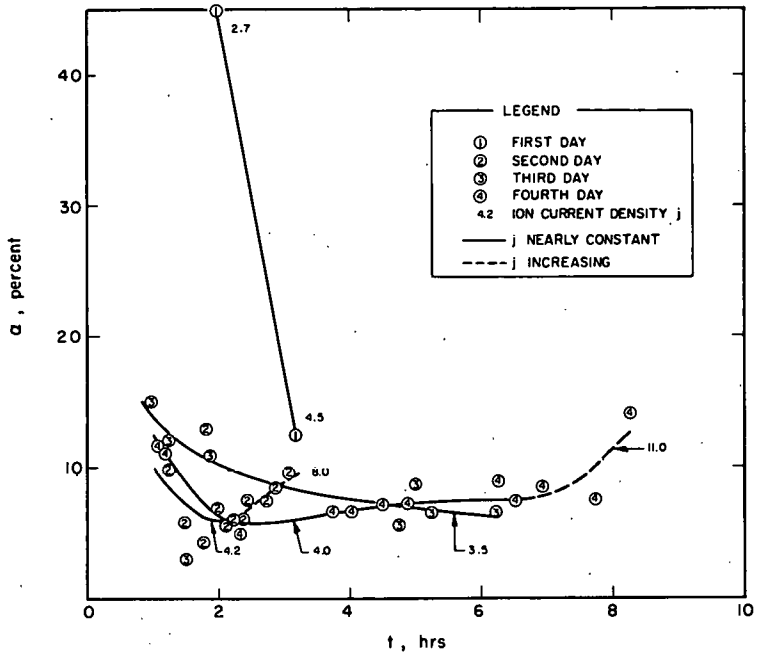


FIG. 31

TIME DEPENDENCE OF NEUTRAL FRACTION SW 5, A = .157 $cm^2$

at high temperatures and the appearance of small surface cracks. The fine wire bundles made of 6 micron diameter wire had much lower neutral fractions than the coarse wire bundles, after an initial conditioning period of about 1-2 hours.

## 10. COMPARISON OF COMMERCIAL, SPHERICAL POWDER AND WIRE BUNDLE IONIZERS

In Fig. 32, surface photomicrographs show the pore sizes and distances for typical ionizers of each type. The commercial porous tungsten has irregular pore sizes and shapes with an equivalent diameter of 2.4 microns, and an average pore distance of 6.7 microns. The spherical powder ionizers have more regular slitlike pores with areas for which the equivalent diameter is 6.4 microns. The average pore distance, assuming a regular distribution into a hexagonal close packed array is 13.5 microns. The coarse wire bundle has some very large pores of about 15 microns with an average of about 4 microns. For most coarse WB ionizers made of 0.0005" dia wire the wire ends were expanded mechanically at the surface to reduce the pore size and produce uniform packing. Operation at high temperature tended to open up the pores. The fine wire bundle made of 0.00025" dia wire had a 0.3 micron equivalent pore diameter.

The apparent nitrogen permeability of all ionizers was compared in Table III. The average SP ionizer was about 4 times, the average WB ionizer about 10 times more permeable to nitrogen than the average SW ionizer. The cesium conductance at operating temperature as given by the atom efflux measurements in Fig. 8 and by ion current density in Fig. 9 follow a similar pattern but the spread is larger for the atom detector data and smaller for the ion current density data. No accurate correlation of nitrogen and cesium permeability has been attempted since this information has been of secondary importance and is dependent upon uncertainties in the reservoir temperature measurement effects of elevated ionizer temperatures. The change of permeability with the ionizer

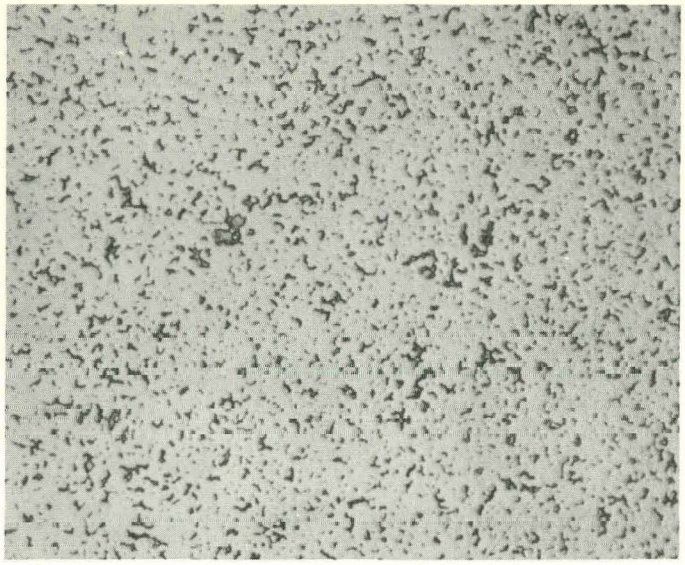

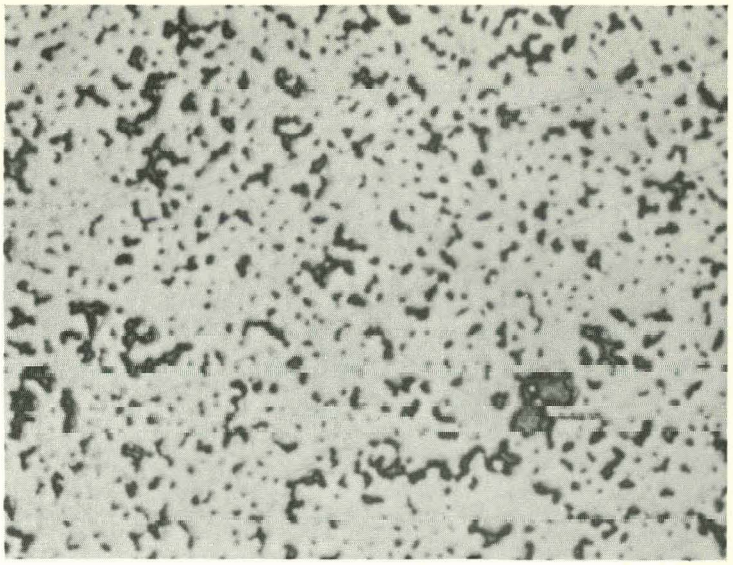

COMMERCIAL POROUS TUNGSTEN

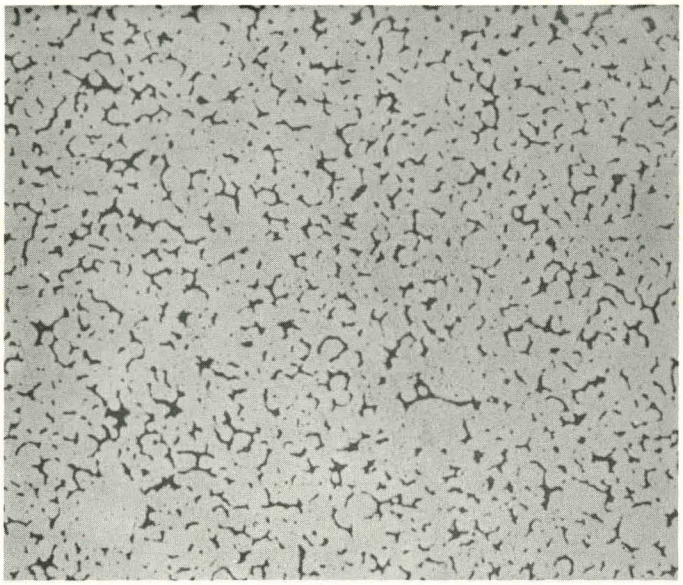

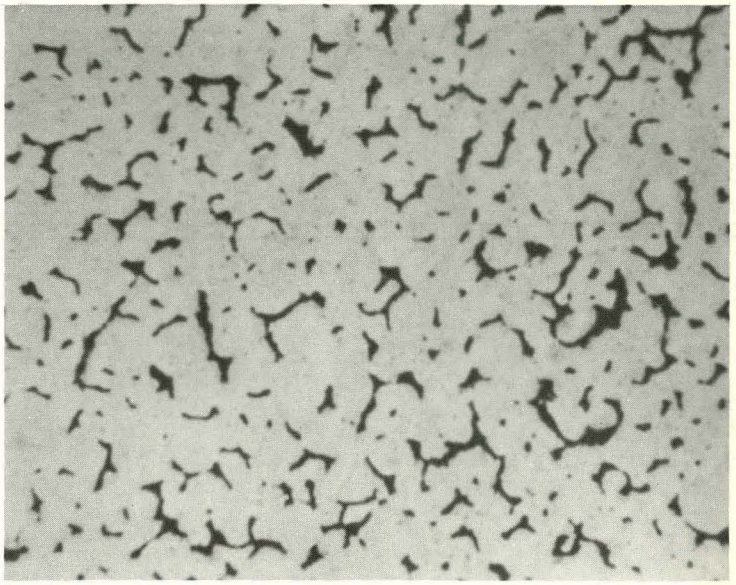

SPHERICAL POWDER

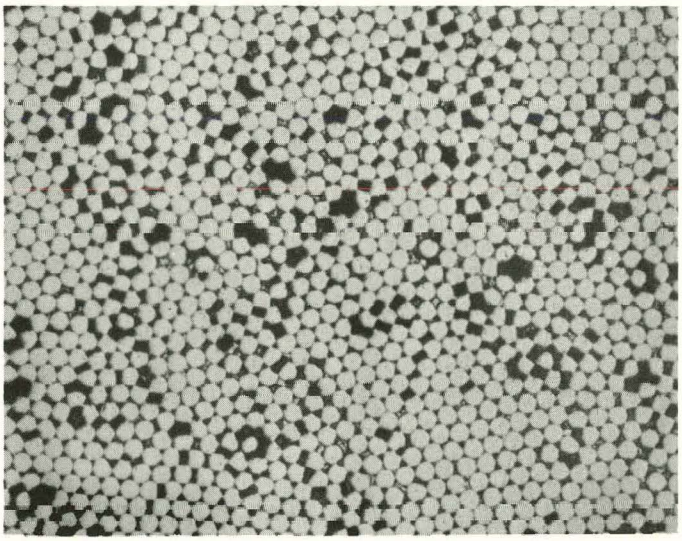

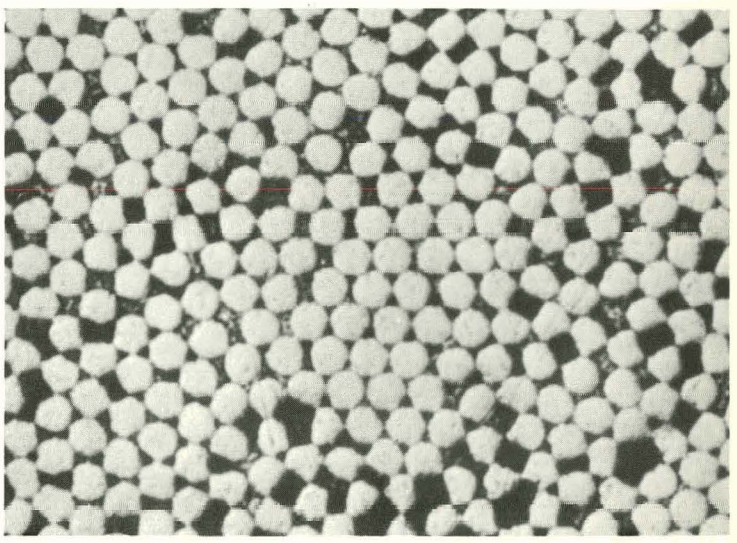

WIRE BUNDLE

FIG. 32 SET OF COMPARATIVE SURFACE PHOTOMICROGRAPHS

temperature was about 3%/100°K for all structures.

The angular distributions of atoms indicated evaporation from the surface for SW ionizers and mostly from the surface for WB ionizers with small pore sizes or from within the pores for WB ionizers with large pore sizes.

The critical temperatures of all SP ionizers given in Fig. 26 demonstrate the spread of points from sample to sample and the differenee between $T_{CI}$ and $T_{C\alpha}$. Such differences were not observed for the SW ionizers in Fig. 27 or for most of the 12 micron wire bundles as in Fig. 28. A very pronounced minimum was observed in $\alpha$ at $T_{C\alpha}$ which was very nearly equal to $T_{CI}$ for the 6 micron wire bundle in Fig. 29.

A comparison of current vs critical temperature, $T_{CI}$, data for all tungsten structures with data published by other investigators is given in Fig. 33. Nearly all tungsten ionizers fall within a band which is between about 30° and 130°K above the Langmuir line. The data taken during initial conditioning periods are neglected. The spread for SP and WB ionizers is smaller (about 90°K) as compared to the SW ionizers. With the exception of data by Husmann, all ionizer surfaces are expected to be oxygenated.

Similar distributions of points are found in the $\alpha$ vs j data of Fig. 29. These same data are summarized and compared with results of other investigators in Fig. 34. The coarse wire bundle ionizers had very high neutral fractions and the commercial porous tungsten showed a very large spread. The spherical powder ionizers had a narrow spread with values similar to the fine wire bundle. The highest ion current density was reached with the SP ionizers, the fine wire bundle being next highest. Again all data, except the band due to Hussman and marked SW-clean, was obtained at $10^{-6}$ torr residual gas pressure where the surfaces are probably oxygenated.

A tabular summary of data on all commercial sintered tungsten ionizers is given in Table IV, for all spherical powder ionizers

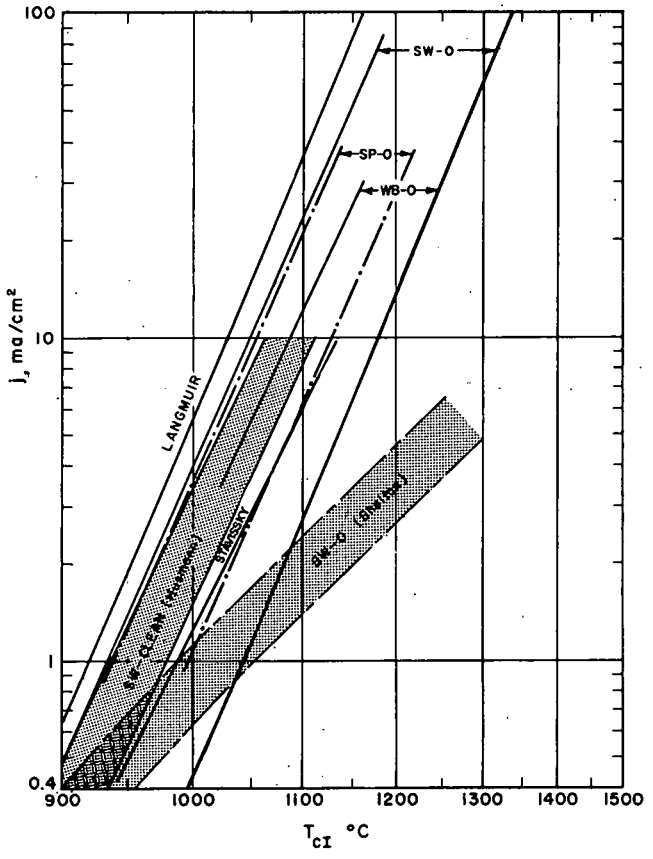


FIG. 33

COMPARISON OF CRITICAL TEMPERATURES FOR
1) BUNDLE IONIZERS
2) SPHERICAL POWDER
3) WIRE BUNDLE IONIZERS

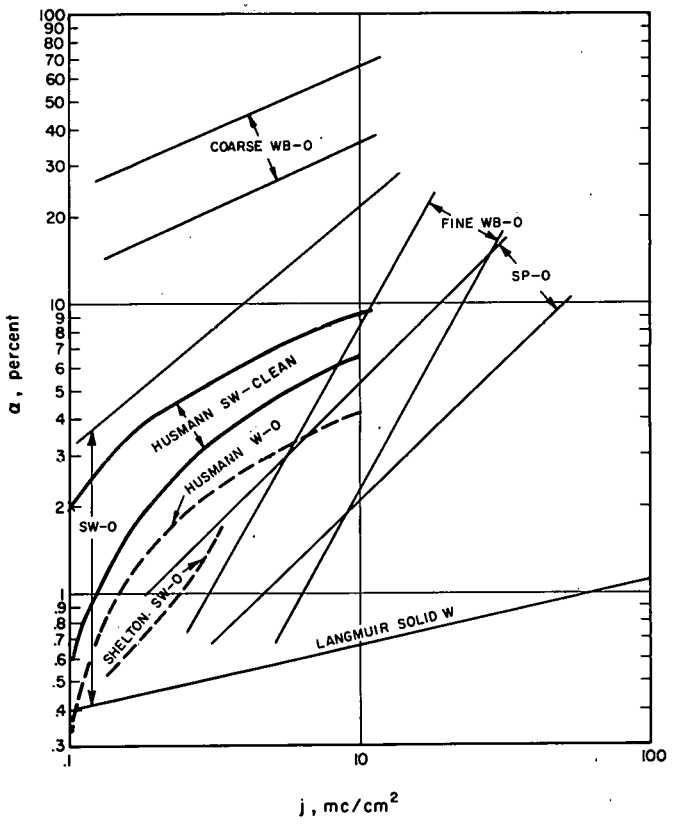


FIG. 34

COMPARISON OF NEUTRAL FRACTIONS OF THE VARIOUS TUNGSTEN STRUCTURES WITH RESULTS OF OTHER INVESTIGATIONS

in Table V and for all wire bundle ionizers in Table VI. Performance tests are continuing and some ionizers of each type will be tested at lower residual gas pressures in an ultrahigh vacuum system. The more regular structures, such as the fine wire bundle and the spherical powder ionizers have given better performance than the commercial sintered tungsten but a final comparison should include data on more samples and at lower residual gas pressures.

TABLE IV

PERFORMANCE DATA FOR COMMERCIAL SINTERED TUNGSTEN IONIZERS

| | | SW1 | SW2 | SW3 | SW4 | SW5 | SW6 | SW7 |
|---|---|---|---|---|---|---|---|---|
| K | Button only | - | - | - | - | - | .46 | 1.7 |
| $\left(\frac{g \times 10^{-6}}{cm \cdot torr \cdot sec}\right)$ | After brazing | 0.078 | .119 | .392 | 0.186 | 0.257 | - | 0.570 |
| | After testing | 0.101 | 0.111 | .227 | 0 | .345 | .285 | 0.506 |
| j at | 300°C | 2.5 | 2 | .9 | | 1.6 | 2.7 | 6.0 |
| | 400°C | (9) | 10.5 | (6) | | 9 | (16) | (53) |
| $T_r$, °C | 5 ma/cm$^2$ | 365 | 355 | 395 | | 360 | 335 | 295 |
| | 20 ma/cm$^2$ | (460) | (450) | | | (430) | (415) | (350) |
| j max | ma/cm$^2$ | 5.2 | 12.5 | 5.6 | | 11.0 | 11 | 8.6 |
| safe | " | 5 | 12 | | | | 11 | 8.6 |
| $\alpha$(low-high) | at 5 ma/cm$^2$ | .1-6 | .2 | 8-13 | | 3-8 | .1-1 | .2-.5 |
| | 20 ma/cm$^2$ | | | | | | | |
| $(T_{CI}-T_L)$°C | Initial | 150 | 65 | | | 250 | 250 | 40 |
| | Low | 20 | 15 | | | 110 | -5 | 25 |
| | High | 110 | 65 | | | 200 | 150 | 40 |
| | Average | 50 | 30 | | | 175 | 100 | |
| Avg. interception at 10 ma/cm$^2$ = 100 $I_a/I_e$ | | 5-10 | - | - | - | 25-45 | 2.5-10 | 15-20 |
| Total Area, cm$^2$ | | .244 | .179 | .179 | .179 | .179 | .179 | .179 |
| Active Area, cm$^2$ | | (.216) | (.157) | (.157) | (.157) | (.157) | (.157) | (.157) |

Numbers in parentheses are extrapolated.

TABLE V

PERFORMANCE DATA FOR SPHERICAL POWDER IONIZERS

| | | SP1 | SP2 | SP3 | SP4 |
|---|---|---|---|---|---|
| K $\left(\frac{g \times 10^{-6}}{cm \cdot torr \cdot sec}\right)$ | Button only | 1.42 | .92 | 1.17 | 1.17 |
| | After brazing | .367 | .495 | .628 | .553 |
| | After testing | .473 | .633 | .624 | .535 |
| j at | 300°C | 3.5 | 4.3 | 3.7 | 1.3 |
| | 400°C | (25) | (34) | (27) | (26) |
| $T_r$ °C | 5 ma/cm$^2$ | 318 | 305 | 312 | 340 |
| | 20 ma/cm$^2$ | 388 | 370 | (383) | (390) |
| j max ma/cm$^2$ | | 20 | 29 | 18 | 13 |
| safe " | | 17 | 18 | 18 | 13 |
| $\alpha$(low-high at 5 ma/cm$^2$ | | 1-2 | .1-2 | | |
| 20 ma/cm$^2$ | | 2-5 | 8-10 | | |
| $(T_{CI}-T_C)$°C | Initial | 50 | 0 | 5 | 95 |
| | Low | 150 | -30 to -20 | 70 | 120 |
| | High | 150 | 71 | 70 | 120 |
| | Average | 60 | 30 | 30 | |
| Avg."interception"at 10 ma/cm$^2$ = 100 $I_a/I_E$ | | 10 | 40 | 5 | |
| Total Area, cm$^2$ | | .178 | .178 | .178 | .178 |
| Active Area, cm$^2$ | | (.157) | (.157) | (.157) | (.157) |

Numbers in parentheses are extrapolated.

TABLE VI PERFORMANCE DATA OF TUNGSTEN WIRE BUNDLE IONIZERS

| Wire Size | | 12 μ | | | | | | 6 μ |
|---|---|---|---|---|---|---|---|---|
| | | WB1J | WB2J | WB1 | WB2 | WB3 | WB4 | WB5 | WB6 |
| K $\left(\frac{g \times 10^{-6}}{cm \cdot torr \cdot sec}\right)$ | Button only | | | | | | | | |
| | After brazing | | 3.48 | 1.41 | 1.38 | 2.90 | 3.34 | | 3.04 |
| | After testing | | 3.59 | 3.73 | | | 5.82 | .225 | 3.27 |
| j at 300°C | | | (14) | | (7) | (17) | (12) | (13) | 24 |
| 400°C | | | | | | | | | |
| $T_r$, °C | 5 ma/cm$^2$ | 227 | 265 | | 275 | 238 | 253 | 225 | 240 |
| | 20 ma/cm$^2$ | | | | | | | | 290 |
| j max ma/cm$^2$ | | 7.5 | 9.0 | 5.3 | 4.8 | 10 | 2.1 | 10 | 29 |
| safe " | | 6 | 7 | 4 | 4 | 6 | 1.5 | | 29 |
| α(low-high) at 5 ma/cm$^2$ | | - | - | 20-44 | 20-46 | 5-48 | 19-40 | 7 | .6-1.5 |
| 20 ma/cm$^2$ | | - | - | - | - | - | - | - | 7-10 |
| $(T_{CI}-T_L)$°C | Initial | | | - | | 75 | | | 125 |
| | Low | | | 75 | | 40 | | | 100 |
| | High | | | 150 | | 120 | | | 175 |
| | Average | | | 100 | | 100 | | | 150 |
| Avg. interception at 10 ma/cm$^2$ = 100 $I_a/I_E$ | | 250 | 73 | 100 | 15 | 200 | | 10 | |
| Total Area, cm$^2$ | | .079 | .079 | .178 | .178 | .178 | .178 | .178 | .148 |
| Active Area, cm$^2$ | | (.079) | (.079) | (.141) | (.141) | (.141) | (.141) | (.141) | .114 |

Numbers in parentheses are extrapolated.

## REFERENCES


Ap59ZI E. Ya. Zandberg and N. I. Ionov, "Surface ionization", Usp. Fiz. Nauk 67 No. 2, pp. 581-623 (Apr. 1959)

Mr62KS4 G. Kuskevics, R. C. Speiser, R. M. Worlock and D. Zuccaro, "Ionization, emission and collision processes in the cesium ion engine", ARS Electric Prop. Conf., Berkeley, No. 2364-62, 42 p. (Mar. 14-16, 1962)

De58BD6 G. Baldwin, R. D. Downing, R. F. Edgar, E. E. Goodale, J. F. Lawyer and L. H. Stauffer, "Experimental investigation pertinent to an ionic propulsion concept", GE R. No. 58GL355, p. 144, (Dec. 26, 1958).

Au59FS A. T. Forrester and R. C. Speiser, "Design criteria for ion rockets", Rocketdyne Res. R. No. 59-30, 45 p. (Aug. 18, 1959)

No60ZST D. Zuccaro, R. C. Speiser and J. M. Teem, "Characteristics of porous surface ionizers", ARS Electrost. Prop. Conf., Monterey, Calif., No. 1387-601, 30 p., (Nov. 3-4, 1960); Electrost. Prop., Acad. Press, 1961, pp. 107-139).

No60NS G. M. Nazarian and H. Shelton, "Theory of ion emission from porous media", ARS Electrost. Prop. Conf., Monterey, Calif., No. 1386-60, 19 p., (Nov. 3-4, 1960)

Au61RK T. W. Reynolds and L. W. Kreps, "Gas flow, emittance and ion current capabilities of porous tungsten", NASA TN D-871, 43 p., (Aug. 1961)

Oc60SL Yu. Ya. Stavissky and S. Ya. Lebedev, "Surface ionization of cesium upon diffusion through porous tungsten", Zh. Tekh. Fiz. 30, No. 10, pp. 1222-1226, (Oct. 1960), Sov. Phys.-Tech. Phys. 5, No. 10, pp. 1158-1161, (Feb. 1961)

Mr62Hus O. K. Husmann, "Experimental evaluation of porous materials for surface ionization of cesium and potassium", ARS Electric Prop. Conf., Berkeley, No. 2359-62, (March 14-16, 1962)

REFERENCES cont.


Au61HRL Hughes Research Lab ., "Design, fabrication and testing of a cesium ion rocket engine - Phase II", NASA Contr. No. NAS5-517, Per: Sept. 1, 1960 - Aug. 31, 1961, FR, 188 p., (Aug. 31, 1961)

My62HRL Hughes Research Lab, "Design, fabrication and testing of a cesium ion rocket engine - Phase II", NASA Contr. No. NAS5-517 Per: Mar. 1, 1962 - May 31, 1962, QPR No. 3, 85 p. (May 31, 1962)

No61HRL Hughes Research Lab., "Design, fabrication, and testing of a cesium ion rocket engine - Phase II", NASA Contr. No. NAS5-517, Per: Sept. 1, 1961 - Nov. 30, 1961, QPR No. 1, 59 p., (Nov. 1961)

Jn61HS R. A. Hubach and G. D. Seele, "Properties of porous tungsten and ionization of cesium", Nat. IAS-ARS Joint Mtg., Los Angeles, No. 61-86-1780, 53 p., (June 13-16, 1961)

Ja62Kus G. Kuskevics, "Criteria and a graphical method for optimization of cesium surface ionizer materials", EOS R. No. RR-3, Jan. 1962. Submitted to the Journal of AIAA

33TL J. B. Taylor and I. Langmuir, "The evaporation of atoms, ions and electrons from cesium films on tungsten", Phys. Rev. 44, p. 423 (1933)